

Braneworld resonances

Chris Clarkson* and Sanjeev S. Seahra†

Institute of Cosmology & Gravitation, University of Portsmouth, Portsmouth, PO1 2EG, UK

(Dated: March 14, 2018)

We investigate in detail gravitational waves in an Schwarzschild-anti-de Sitter bulk spacetime surrounded by an Einstein static brane with generic matter content. Such a model provides a useful analogy to braneworld cosmology at various stages of its evolution, and generalizes our previous work [gr-qc/0504023] on pure tension Einstein-static branes. We find that the behaviour of tensor-mode perturbations is completely dominated by quasi-normal modes, and we use a variety of numeric and analytic techniques to find the frequencies and lifetimes of these excitations. The parameter space governing the model yields a rich variety of resonant phenomena, which we thoroughly explore. We find that certain configurations can support a number of lightly damped ‘quasi-bound states’. A zero-mode which reproduces 4-dimensional general relativity is recovered on infinitely large branes. We also examine the problem in the time domain using Green’s function techniques in addition to direct numeric integration. We conclude by discussing how the quasi-normal resonances we find here can impact on braneworld cosmology.

I. INTRODUCTION

Resonant states play a pivotal role in understanding many physical systems from drums to molecules to black holes [1]. They often take centre stage because they contain the key observable features that are characteristic of the physical system, irrespective of the initial conditions that excite them in the first place. Braneworlds, it appears, are no different [2, 3]. Even though a system may be infinite and therefore unable to support a countable collection of normal modes, there may exist discrete complex frequencies which are nevertheless preferentially excited by initial data – so-called ‘quasi-normal modes’ (QNMs). The real parts of these frequencies are typically dependent on the length scale of the system, while the imaginary part tells us the rate at which energy is lost to infinity in each particular mode. A recent investigation [2] has shown how the one-brane Randall-Sundrum (RS) model [4] exhibits exactly this behaviour: the continuous Kaluza-Klein (KK) spectrum of gravitons has preferential masses with very short lifetimes.

Such resonant phenomena may have a significant effect in braneworld cosmology.¹ As is well known, the effective 4-dimensional formalism governing perturbations on the brane is not closed; that is, there are dynamical degrees of freedom on the brane whose evolution is determined by non-local bulk effects. Any complete picture of braneworld cosmology must include these degrees of freedom, but this is notoriously difficult to implement in practice. Limiting the discussion to one-brane models, we note that some progress has been made in certain special cases [6, 7, 8, 9, 10], by using various approximation schemes [11, 12, 13, 14, 15, 16, 17, 18, 19], and

direct numeric solution of the problem in 5 dimensions [20, 21, 22, 23].

An alternative line of attack arises from realizing that the behaviour of perturbations will be dominated by resonances of the brane-bulk system, which are precisely the quasi-normal modes. Given knowledge of the nature of these resonances, one should be able to make reasonable predictions about the effect bulk gravity waves have on the brane without knowing the details of how they were generated. This is especially useful since the correct initial conditions for bulk gravity waves in such models are not really known.

There are two aspects to the quasi-normal mode problem for cosmological branes: the nature of the bulk, and the motion of the brane. The latter is tricky because of the non-separability of the equations of motion (the boundary condition in particular). However, a static configuration is relatively straightforward, and is a useful approximation to a cosmological model provided the brane motion is ‘slow’.

A Friedmann-Lemaître-Robertson-Walker brane may exist in a 5-dimensional bulk provided that it is a piece of Schwarzschild-anti-de Sitter (S-AdS₅) [5]. We shall focus on the case of a positive curvature S-AdS₅, with an Einstein static brane around it, and choose the ‘inside’ part of the bulk (i.e., including the black hole), while enforcing \mathbb{Z}_2 symmetry across the brane. In a previous paper [3] we have investigated tensor perturbations when the brane is pure tension. In this situation we found that gravity is ‘delocalized’: gravity is sucked off the brane by the presence of the black hole, removing the GR-like zero-mode. Moreover, the presence of quasi-normal modes was investigated and were shown to be quite heavily damped, but with a mass-gap between the fundamental mode and the higher overtones.

The pure tension condition, while useful for comparison with RS models, forces the brane to be located at the photon sphere of the bulk, providing only a glimpse of the possible range of behaviour relevant to cosmology. In particular, if the brane is moving it will pass, in princi-

*Electronic address: chris.clarkson@port.ac.uk

†Electronic address: sanjeev.seahra@port.ac.uk

¹ See Ref. [5] for a comprehensive review of all aspects of braneworld gravity.

ple, from the white hole region through the horizon and out to infinity (or maybe re-collapse). Hence we shall consider all brane locations outside the horizon.

In this paper we show that the gravity waves are indeed dominated by quasi-normal modes, the character of which depend strongly on the brane location. Roughly speaking, the closer the brane to the black hole horizon the higher the imaginary parts of the QNMs: this corresponds to the stronger gravity of the black hole draining gravitons of the brane more effectively. On the other hand, for branes located far from the black hole, or on small scales on the brane (provided the black hole mass is not too large compared to the AdS length scale), the damping of the modes is so small that the gravitons are effectively confined to the region between the brane and the photon sphere of the black hole: in effect, the quasi-normal modes become (approximate) normal modes, and gravity waves behave akin to two-brane scenarios. Thus, we find what we are looking for: brane signals are effectively ‘combed’ in the frequency domain to be composed of a discrete spectrum of *very* lightly damped harmonic modes – sharp evenly spaced spikes. Somewhat regardless of the initial data, these spikes are the main feature of the signal on the brane.

The layout of the paper is as follows: In Section II we discuss the Einstein static brane in S-AdS₅, and tensor perturbations therein. In Section III we consider a qualitative wave-mechanics analysis of the problem, before going on to calculate QNMs for these models using a series solution for the master wave equation. This technique proves to be computationally intensive for brane locations far from the horizon, so in Section IV we use an alternative approach for finding QNMs with small imaginary parts – which we call *quasi-bound states*. We then undergo a detailed study of how these states behave in the three dimensional parameter space which governs these models. We then discuss the utility of our results in the time domain in Section V using both analytic Green’s function and numerical methods. We find the existence of coherent states which would look like bouncing gravitons to a brane observer; we also consider Hawking radiation, and its distorted spectrum on the brane. Finally in Section VI we summarise our results and consider the implications for cosmology.

II. THE EINSTEIN-STATIC BRANEWORLD

A. Bulk geometry

The bulk geometry of the brane universes considered in this paper are given by the Schwarzschild-AdS₅ line element, which is conventionally written as:

$$ds_{(5)}^2 = -f dT^2 + f^{-1} dR^2 + R^2 d\Omega_3^2, \quad (1a)$$

$$f = 1 - \frac{R_0^2}{R^2} + \frac{R^2}{\ell^2}. \quad (1b)$$

Here, R_0 is related to the ADM mass of the black hole while ℓ is related to the (negative) cosmological constant. It is convenient to rewrite f as

$$f = \frac{(R^2 + R_h^2 + \ell^2)(R^2 - R_h^2)}{R^2 \ell^2}, \quad (2)$$

where

$$R_h^2 = \frac{\ell^2}{2} \left(\sqrt{\frac{4R_0^2}{\ell^2} + 1} - 1 \right). \quad (3)$$

When the solution is written in this way, it is obvious that there is an event horizon at $R = R_h$. For simplicity, we will use dimensionless (t, r) coordinates defined by the substitutions:

$$\begin{aligned} R &\rightarrow r \times R_h, \\ \mathcal{T} &\rightarrow t \times R_h, \\ ds_{(5)}^2 &\rightarrow ds_{(5)}^2 \times R_h^2. \end{aligned} \quad (4)$$

In terms of these quantities, the bulk line element looks like

$$ds_{(5)}^2 = -f dt^2 + f^{-1} dr^2 + r^2 d\Omega_3^2, \quad (5a)$$

$$f(r) = \frac{(r^2 + \gamma^2 + 1)(r^2 - 1)}{\gamma^2 r^2}, \quad \gamma \equiv \frac{\ell}{R_h}. \quad (5b)$$

In this representation, the bulk geometry is completely characterized by the ratio of the AdS length scale to the horizon radius of the black hole γ and the horizon is always at $r = 1$. We shall call solutions with $\gamma \lesssim 1$ ‘big’ black holes and solutions with $\gamma \gtrsim 1$ ‘small’ black holes. In order to reintroduce dimensions to any quantity in the (t, r) coordinates, one has to multiply by the appropriate power of the horizon radius R_h .

B. Einstein-static branes and their matter content

An Einstein-static brane is introduced by identifying some $r = r_b$ as the boundary Σ_0 of the 5-manifold and discarding the portion with $r > r_b$. The brane geometry is then simply that of an Einstein static universe:

$$ds_{(4)}^2 = -d\tau^2 + r_b^2 d\Omega_3^2, \quad (6)$$

where $\tau = f(r_b)t$ is the cosmic time. The normal to Σ_0 is selected to point *away* from the brane and is obtained by evaluating the following at $r = r_b$:

$$n_a = -f^{-1/2} \partial_a r. \quad (7)$$

With this normal, one finds that the extrinsic curvature of Σ_0 is

$$K_{ab} = h^c{}_b \nabla_c n_a = -\frac{1}{2f^{1/2}} \frac{df}{dr} u_a u_b - \frac{f^{1/2}}{r} q_{ab}, \quad (8)$$

where evaluation at $r = r_b$ is understood. Here, we have defined the objects

$$u_a = -f^{1/2}\partial_a t, \quad (9a)$$

$$h_{ab} = g_{ab} - n_a n_b, \quad (9b)$$

$$q_{ab} = h_{ab} + u_a u_b; \quad (9c)$$

where u^a is the future-directed normal to constant t surfaces, h_{ab} is the induced 4-metric on the brane, and q_{ab} is the spatial 3-metric.

The matter content of the brane is determined as follows: First, assume a brane stress energy tensor of the perfect fluid form

$$S_{ab} = \rho_{\text{tot}} u_a u_b + p_{\text{tot}} q_{ab}. \quad (10)$$

The fluid quantities ρ_{tot} and p_{tot} refer to the total brane density and pressure, including any contribution from the brane tension σ . Hence, these can be further decomposed as

$$\rho_{\text{tot}} = \rho_m + \kappa^{-1}\sigma, \quad p_{\text{tot}} = p_m - \kappa^{-1}\sigma, \quad (11)$$

where κ is a dimensionless 5-dimensional gravity-matter coupling constant, while ρ_m and p_m refer to the density and pressure of ‘ordinary’ brane matter. Imposing \mathbb{Z}_2 reflection symmetry across the brane yields (via the standard junction conditions):

$$\kappa S_{ab} = -2(K_{ab} - K h_{ab}), \quad (12)$$

which is then equivalent to

$$K_{ab} = -\kappa \left(\frac{1}{3}\rho_{\text{tot}} + \frac{1}{2}p_{\text{tot}} \right) u_a u_b - \frac{1}{6}\kappa\rho_{\text{tot}}q_{ab}. \quad (13)$$

Comparison of (8) and (13) yields the following consistency conditions for an Einstein static brane:

$$\left. \frac{1}{f^{1/2}} \frac{df}{dr} \right|_{r=r_b} = -2\kappa \left(\frac{\rho_{\text{tot}}}{3} + \frac{p_{\text{tot}}}{2} \right), \quad (14a)$$

$$\left. \frac{f^{1/2}}{r} \right|_{r=r_b} = \frac{\kappa\rho_{\text{tot}}}{6}. \quad (14b)$$

It is possible to derive these conditions from the effective Friedman equation governing a general brane universe embedded in S-AdS₅:

$$\frac{\dot{a}^2}{a^2} = -\frac{f(a)}{a^2} + \frac{\kappa^2\rho_{\text{tot}}^2}{36}, \quad (15)$$

where an overdot indicates differentiation with respect to cosmic time. A time derivative of (15) yields the Raychaudhuri equation for \dot{a} , and setting $\dot{a} = \ddot{a} = 0$ yields (14) when the first law $d(\rho_{\text{tot}}a^3) = -p_{\text{tot}}d(a^3)$ is enforced and the identification $a = r_b$ is made.

Equations (14) comprise a system of 2 equations in 4 variables $\{\gamma, r_b, \rho_{\text{tot}}, p_{\text{tot}}\}$. Hence, there is a 2-parameter family of Einstein-static brane solutions. For our purposes it is useful to regard the size of the bulk black hole γ and the brane position r_b as free parameters, while the

matter characteristics $\{\rho_{\text{tot}}, p_{\text{tot}}\}$ are inferred from (14). It is easy to show that for the restrictions $\gamma > 0$ and $r_b > 1$, there is always a solution for $\{\gamma, r_b, \rho_{\text{tot}}, p_{\text{tot}}\}$. Furthermore, the effective equation of state of the brane matter is

$$w_{\text{tot}} \equiv \frac{p_{\text{tot}}}{\rho_{\text{tot}}} = -\frac{3r_b^4 - \gamma^2 - 1 + 2\gamma^2 r_b^2}{3(r_b^2 + \gamma^2 + 1)(r_b^2 - 1)} < -\frac{2}{3}. \quad (16)$$

The inequality implies that a necessary condition for an Einstein-static brane universe is $2\rho_{\text{tot}} + 3p_{\text{tot}} < 0$. In other words, the total brane matter distribution must violate the 5-dimensional version of the strong energy condition. This makes sense since the brane is essentially a static shell of matter around a black hole. The only way to maintain such a configuration is to construct the shell out of gravitationally repulsive material, hence the violation of the strong energy condition. Note that does not necessarily hold for the non-tension contribution to $\{\rho_{\text{tot}}, p_{\text{tot}}\}$; i.e., it is possible to have $\{\rho_m, p_m\}$ consistent with the energy conditions depending on the choice of σ .

Our principle concern is to understand how gravity waves change with brane location. If the brane were allowed to move, these conditions would no longer apply for a given brane position.

C. Tensor perturbations

We now consider tensor perturbations of the bulk using the general results of Kodama and Ishibashi [24] specialized to S-AdS₅. Under such fluctuations:

$$g_{ab} \rightarrow g_{ab} + \delta q_{ab}, \quad u^a \delta q_{ab} = n^a \delta q_{ab} = 0, \quad (17)$$

where δq_{ab} is the perturbed spatial 3-metric.

The SO(4) bulk symmetry allows a mode decomposition of δq_{ab} in terms of tensor harmonics on the unit 3-sphere S^3 . Let $i, j = 1, 2, 3$ and ∇_i be the metric-compatible covariant derivative on S^3 . Then, tensor harmonics are defined by

$$\square \mathbb{T}_{ij}^{(k)} = -k^2 \mathbb{T}_{ij}^{(k)}, \quad \nabla^i \mathbb{T}_{ij}^{(k)} = 0 = \text{Tr } \mathbb{T}^{(k)}, \quad (18)$$

where $\square = \nabla^i \nabla_i$, and

$$k^2 = L(L+2) - 2, \quad L = 1, 2, 3, \dots \quad (19)$$

Now, if θ^i are suitable angular coordinates on S^3 , the harmonic decomposition of the metric perturbation reads:

$$\delta q_{ab} = \partial_a \theta^i \partial_b \theta^j \sum_k r^{1/2} \psi_k(t, r) \mathbb{T}_{ij}^{(k)}. \quad (20)$$

When this is substituted into the linearized Einstein equations, one finds that each of the ψ_k satisfies a wave equation

$$-\frac{\partial^2 \psi_k}{\partial t^2} = -\frac{\partial^2 \psi_k}{\partial x^2} + V_k(r) \psi_k, \quad x = x(r) \equiv \int \frac{du}{f(u)}, \quad (21)$$

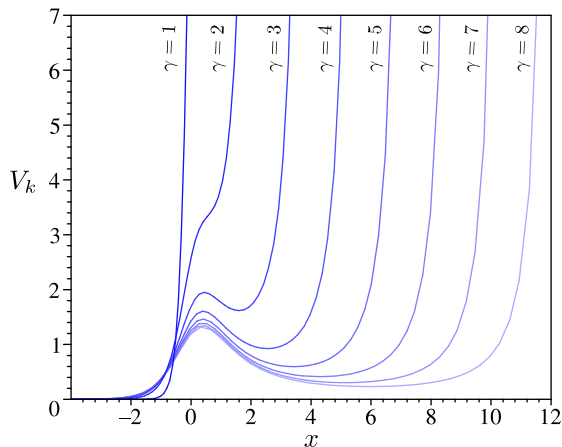


FIG. 1: The potential in the master equation governing tensor perturbations in S-AdS₅ with no brane present and $L = 1$

where x is the tortoise coordinate and the potential is

$$V_k(r) = f \left[\frac{15}{4\gamma^2} + \frac{4k^2 + 11}{4r^2} + \frac{9(\gamma^2 + 1)}{4\gamma^2 r^4} \right]. \quad (22)$$

The $L = 1$ potential is shown in Figure 1 for several values of γ . We see that for large γ , there is a barrier near $x = 0$ and an infinite wall at some finite $x > 0$. For small γ the barrier is absent, but the wall is still there. The form of V_k highlights one of the curious properties of AdS space, namely $r(x) \rightarrow \infty$ at a finite value of x . This means that, unlike asymptotically flat spacetimes, it is possible for gravity wave, electromagnetic, or other types of signals to propagate from finite r to $r = \infty$ in a finite amount of coordinate time. The infinite walls of the potential curves in Figure 1 indicate the x position of spatial infinity, and in the absence of a brane one needs to specify boundary conditions there to have a well-posed Cauchy problem for the evolution of ψ_k .

But we are interested in the case where there is a brane and the asymptotic region is not there, so we need the boundary condition on tensor perturbations at the brane location. To find this, we need to introduce 4-dimensional coordinates y^α , where the $\alpha, \beta \dots$ indices run over the directions tangent Σ_0 . Then, 4-tensors are related to 5-tensors by

$$T_{\alpha\beta} = \partial_\alpha x^a \partial_\beta x^b T_{ab}, \text{ etc.} \quad (23)$$

In the background geometry, the fact that the radial off-diagonal metric elements $g_{r\alpha}$ are zero imply

$$K_{\alpha\beta} = -\frac{1}{2} f^{1/2} \partial_r h_{\alpha\beta}. \quad (24)$$

Since tensor fluctuations have $n^a \delta g_{ab} = 0$, this formula

also holds after perturbation.² Hence,

$$\delta K_{\alpha\beta} = -\frac{1}{2} f^{1/2} \partial_r \delta h_{\alpha\beta} \Rightarrow \frac{\kappa \rho_{\text{tot}}}{3f^{1/2}} \delta q_{\alpha\beta} = \partial_r \delta q_{\alpha\beta}. \quad (25)$$

Then, making use of (14b) to substitute for $\kappa \rho_{\text{tot}} f^{-1/2}$ and simplifying gives

$$0 = \partial_r (r^{-2} \delta q_{\alpha\beta})_{r=r_b}. \quad (26)$$

It is worthwhile to contrast this with the boundary condition for perturbations $\delta h_{\alpha\beta}$ in a Randall-Sundrum model with scale factor $A(y)$ and in the Randall-Sundrum gauge: $\partial_y (A^{-2} \delta h_{\alpha\beta}) = 0$ on the brane. Finally, we use (26) term-by-term in the expansion (20) to obtain the boundary condition satisfied by the master variable:

$$0 = \partial_r (r^{-3/2} \psi_k)_{r=r_b}, \quad (27)$$

which is of a mixed Neumann-Dirichlet type.

III. QUASI-NORMAL GRAVITY WAVE RESONANCES

We have seen in Sec. IIC that tensor perturbations of the Einstein static braneworld are governed by a one-dimensional wave equation (21) subject to a boundary condition (27) at the brane. In this section, we solve this equation via a series solution in order to find the resonant modes of the potential, which are analogous to the quasi-normal modes familiar from black hole perturbation theory.

A. Wave mechanics analysis

If we substitute $\psi_k(t, r) = e^{i\omega t} \Psi_{k\omega}(x)$ into (21), we obtain a time-independent Schrödinger equation,

$$\omega^2 \Psi_{k\omega} = -\Psi_{k\omega}'' + V_k(x) \Psi_{k\omega}, \quad (28)$$

with energy parameter $E = \omega^2$ and a non-standard boundary condition

$$0 = [r^{-3/2}(x) \Psi_{k\omega}(x)]'_{r=r_b}, \quad (29)$$

at the position of the brane. However, this boundary condition can be directly incorporated into the potential via an attractive delta-function. In Fig. 2, we sketch the resulting potential for several different brane positions in the case of a small bulk black hole. There are two qualitatively distinct regimes characterized by the effective equation of state of the brane matter. If this matter has

² An alternative way of saying this is that the vector $r^a = \frac{\partial x^a}{\partial r}$ is parallel to n^a both before and after perturbation.

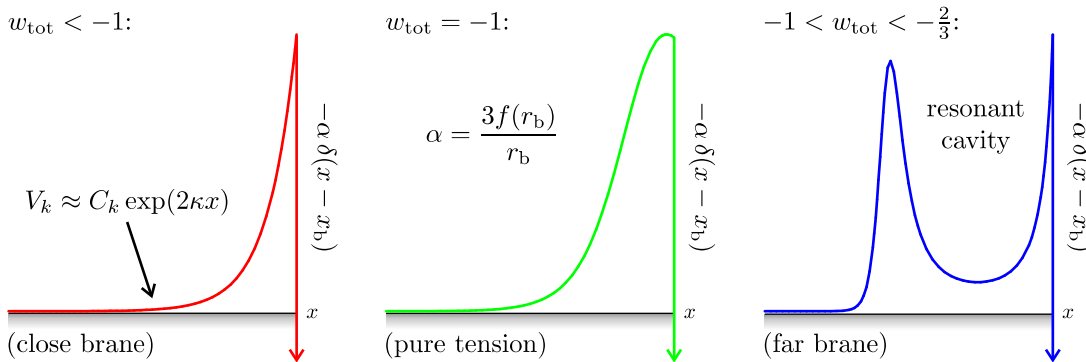


FIG. 2: Tensor gravity wave potentials for various Einstein-static braneworlds with a small bulk black hole. We have taken $\gamma = 10$ and $L = 1$ for these examples

a phantom equation of state $w_{\text{tot}} < -1$, we see that the brane is located in between the bulk black hole’s event horizon and photon sphere. We call this the ‘close brane’ scenario. If the equation of state is more conventional $-1 < w_{\text{tot}} < -\frac{2}{3}$, the brane is located between the photon sphere and spatial infinity. Correspondingly, this is known as the ‘far brane’ scenario. In between the two possibilities is the pure tension case with $w_{\text{tot}} = -1$, when the brane is coincident with the photon sphere.

The qualitative form of the potentials in Fig. 2 can give us valuable clues as to behaviour of gravity waves in the ES braneworld. We see that in all cases, the potential vanishes like $e^{2\kappa x}$ as $x \rightarrow -\infty$; i.e., at the bulk black hole horizon.³ Here, κ is the surface gravity of the black hole:

$$\kappa = \left. \frac{1}{2} \frac{df}{dr} \right|_{r=1} = \frac{2 + \gamma^2}{\gamma^2}. \quad (30)$$

As discussed in detail in Ref. [3], this means we cannot find solutions for Ψ_k with $\omega^2 > 0$ that are localized near the brane. The vanishing of $V_k(1)$ means that the horizon has zero reflectivity; that is, it is a perfect absorber of gravity waves. One cannot construct a stable bound state under such circumstances because there will always be energy leakage into the bulk black hole. This means that there is no Randall-Sundrum like normalizable zero-mode for any Einstein-static braneworld—the bulk black hole essentially delocalizes the brane gravity.

If not stable bound states, what other types of resonances could the potentials in Fig. 2 support? Well, the existence of the attractive delta-function suggests that we may be able to find metastable bound states. There are modes that are ‘almost bound’ to the brane, but are eroded in time by the tunnelling of the wave-function towards the bulk horizon. We can characterize such modes

by a complex frequency with $\text{Im} \omega > 0$; i.e., they are exponentially damped in time. Note that the larger the imaginary part, the higher the damping and the shorter the lifetime. In this sense, they are the equivalent to the familiar quasi-normal modes of black hole perturbation theory. Indeed, metastable bound states are defined entirely analogously to QNMs—namely, they are solutions of the wave equation satisfying ‘purely outgoing’ boundary conditions. In this context, this means that ψ_k satisfies both (27) and

$$\psi_k \sim e^{i\omega(t+x)}, \quad \text{as } x \rightarrow -\infty. \quad (31)$$

Because we are imposing two boundary conditions on a single ODE, it follows that the spectrum of QNM frequencies $\{\omega_i\}$ is discrete. Now, consider the situation where a compact pulse of gravity waves strikes the brane and scatters. A well-known result is that the late-time behaviour of the scattered waveform will be dominated by contributions from QNMs (so-called quasi-normal ringing), independently of the initial data. It is for this reason that it is important to know the quasi-normal frequencies of the brane: they represent the gravitational resonances of the system and hence tend to dominate the gravity wave spectrum seen on the brane.

As an important aside, we note that it is theoretically possible to find QNM solution with $\text{Im} \omega_i < 0$. Such a solution will be spatially normalizable because ψ_k vanishes exponentially as $x \rightarrow -\infty$. It will also be exponentially growing in time, and hence represents an instability of the system. Such an instability would not be unprecedented: It is well known that the 4-dimensional Einstein-static universe is unstable to homogeneous perturbations [25], and that a Schwarzschild black hole enclosed in a finite cavity is unstable to polar perturbations [26] (assuming Dirichlet boundary conditions). This provides another motivation for finding the QNMs of this system; i.e., to determine whether or not it is stable against tensor perturbations.

Before we calculate the quasi-normal frequencies for the Einstein-static braneworld, we comment on the qualitative features of the various small black hole cases shown

³ Though not shown in Fig. 2, the vanishing of the potential at the horizon is true for all values of γ .

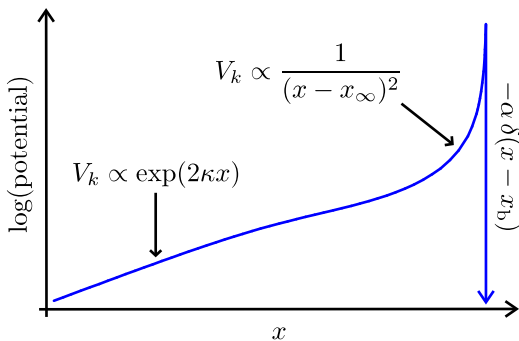


FIG. 3: The tensor potential for a large black hole, far brane ES scenario with $(\gamma, L) = (0.5, 1)$. As in Fig. 2, $\alpha = 3f(r_b)/r_b$ while $x_\infty = x(\infty)$

in Fig. 2. The pure tension potential has been extensively studied in Ref. [3], where it was found that the QNM spectrum featured frequencies whose real and imaginary parts were of the same order. How might we expect this to change for the close and far brane cases? For the far brane case, we see that the peak of the potential and the brane form a kind of finite potential well. It is plausible that gravity waves could be temporarily trapped in this well, but would eventually tunnel out to infinity. We expect a set of QNMs to be associated with this effect, and their real parts should be roughly related to the width of the resonant cavity λ . The trapping efficiency of the cavity will be directly related to the lifetime of the QNMs, and we will see in Sec. IV that the efficiency can be very high indeed, resulting in quasi-normal mode frequencies with tiny imaginary parts.

It is more difficult to guess the behaviour of the QNMs in the close brane limit. This should be considered as the very strong gravity regime, where the delocalizing effects of the black hole horizon are strongest. So we may expect that the imaginary parts of the QNMs to be much larger than the real parts. In this case, the potential is well-approximated by a simple exponential, which allows for an analytic solution that we discuss in Appendix A.

Finally, we comment on the large black hole case. As seen in Fig. 1, there is no clearly defined potential barrier for $\gamma \lesssim 2$, so the far brane resonant cavity we discussed above will not be present for large bulk black holes. The actual far brane potential with γ small is shown in Fig. 3. Near the brane, the potential is proportional to $1/(x - x_\infty)^2$, where x_∞ is the x -coordinate of spatial infinity. The exponential fall-off of the potential as $x \rightarrow -\infty$ is unchanged from the small black hole case, and V_k smoothly interpolates between the two extremes. The lack of a resonant cavity implies that there will be no gravity wave trapping for far branes, but the qualitative features of the near brane and pure tension case should be the same as the small black hole scenario.

B. Series solution

Only so much progress can be made by looking at the potentials in Figs. 2 and 3. So we now turn our attention to an algorithm for actually calculation the quasi-normal frequencies of the ES braneworld. We begin by analyzing the master wave equation (21) in the frequency domain, and transforming the radial coordinate to

$$z = 1 - \frac{1}{r}. \quad (32)$$

This coordinate maps the horizon at $r = 1$ onto $z = 0$ and $r = \infty$ onto $z = 1$. Dropping the k index labelling the different tensor harmonics, we write

$$\psi(t, r) = e^{i\omega t} \phi_\omega(z), \quad (33)$$

which converts (21) into an ordinary differential equation (ODE) of the standard form:

$$\phi_\omega'' + P(z)\phi_\omega' + Q(z)\phi_\omega = 0. \quad (34)$$

where P and Q implicitly depend on ω , γ and L . We will attempt to construct a series solution of the equation, so we need to understand the pole structure of the continuations of P and Q into the complex plane. One finds that $P(z)$ has simple poles at:

$$z = 0, 2, \text{ and } 1 \pm i(\gamma^2 + 1)^{-1/2}. \quad (35)$$

The poles of $Q(z)$ are all of order 2 and are located at:

$$z = 0, 1, 2, \text{ and } 1 \pm i(\gamma^2 + 1)^{-1/2}. \quad (36)$$

From this information, we see that the horizon $z = 0$ and spatial infinity $z = 1$ are regular singular points of the ODE about which we can construct series solutions. Our problem involves discarding the portion of the 5-manifold with $r > r_b$, so we should attempt an expansion about $z = 0$. Our solution will have a radius of convergence greater than or equal to the distance to the closest pole to $z = 0$; i.e., the solution will be valid for $z \in [0, 1]$.

Following the standard procedure, we substitute the ansatz

$$\phi_\omega(z) = z^\varrho \sum_{m=0}^{\infty} a_m z^m \quad (37)$$

into the ODE. The coefficient of the lowest power of z yields an indicial equation with roots:

$$\varrho = \pm \frac{i\gamma^2 \omega}{2(2 + \gamma^2)}. \quad (38)$$

Switching back to the x coordinate, we see that the two possibilities correspond to

$$\phi_\omega \sim e^{\pm i\omega x} \text{ as } x \rightarrow -\infty. \quad (39)$$

Hence, the two signs correspond to waves travelling into or away from the black hole horizon. For a QNM solution we need to choose the former, which is the same as demanding that our perturbation vanishes on the past black hole horizon. Once the sign of ϱ is fixed, it is a straightforward but tedious exercise to obtain a ninth-order recurrence relation for the a_m coefficients.

We have yet to impose the boundary condition at the brane, which is

$$\phi'_\omega(z_b) - \frac{3}{2}r_b\phi_\omega(z_b) = 0, \quad z_b \equiv 1 - 1/r_b. \quad (40)$$

To deal with this, we define an N th order approximation to ϕ_ω via the partial sum:

$$\phi_\omega^{(N)}(z) = z^\varrho \sum_{m=0}^N a_m z^m. \quad (41)$$

Substitution of this into the boundary condition yields an equation $\mathcal{P}_N = 0$, where \mathcal{P}_N is a polynomial of order $2N$ in $i\omega$. Hence, only for a discrete set of $2N$ complex frequencies ω_n will our approximate solution satisfy the brane boundary condition. Now, suppose that in the limit $N \rightarrow \infty$ the roots of the *polynomial sequence* $\{\mathcal{P}_N\}_{N=1}^\infty$ converge to infinite set of discrete frequencies. Then, such a set represents a collection of resonant frequencies of tensor perturbations of the bulk-brane system.

So, the problem of finding resonances for tensor perturbations of Einstein-static braneworld amounts to finding roots of a sequence of polynomials $\{\mathcal{P}_N\}$ that are stable in the $N \rightarrow \infty$ limit. The practical implementation of this scheme is as follows: First, we fix all the input parameters of the problem r_b , L , and γ . Then, we begin with a low order member of $\{\mathcal{P}_N\}$, of degree 30 in ω say, and find all of its roots using Newton's method in the complex plane. Then, we use these roots as initial guesses for Newton's method applied to the polynomial of the next higher order. If Newton's method fails to converge after some number of iterations, we discard the root. But if it does converge, we use the answer as an initial guess for the next order polynomial, and repeat the procedure. We end up with a finite number of roots as a function of N : $\omega_n = \omega_n(N)$. The final step is to reject any of these roots that do not seem to be converging in the $N \rightarrow \infty$ limit; i.e., roots for which the 'convergence factor'

$$\Delta_n(N) = |\omega_n(N) - \omega_n(N-1)|, \quad (42)$$

does not become small for N large. At the end of the day, we are left with a set of resonant frequencies for our choice of r_b , L , and γ .

How big must we make N in order to have accurate answers for $\{\omega_n\}$? There is no entirely straightforward answer, but note that for far branes with $r_b \gg 1$, we have $z_b \rightarrow 1$. This means that we need to evaluate our series solution near the singular point $z = 1$ in order to enforce the boundary condition (40). But we expect

the series to be poorly convergent near a singular point, so in order to satisfy (40) accurately, N must be very large indeed. Hence, to find quasi-normal frequencies for $r_b \gg 1$, we need to retain more and more terms in our approximate answer $\phi_\omega^{(N)}$. This is the principal practical limitation of our method: the computational cost of computing $\{\omega_n\}$ increases dramatically with increasing r_b . Indeed, in Sec. IV we will need to resort to other means to find the resonant modes for r_b very large.

C. Results

In Fig. 4, we plot the several smallest $L = 1$ quasi-normal frequencies of the brane for $\gamma = 20$ and $\gamma = 1/2$. As mentioned above, the maximum value of r_b we can consider is limiting by computing power, so we limit ourselves to the range $r_b \in (1, 5)$. The roots of $\{\mathcal{P}_N\}$ have mirror symmetry about the imaginary axis, i.e., if ω_n is a quasi-normal frequency, then $-\omega_n^*$ is also a solution. Hence, we only plot roots with $\text{Re}\omega_n \geq 0$.

We highlight the key qualitative features:

- In both cases, the QNMs are purely imaginary in the close brane regime, i.e., for $r_b \rightarrow 1$. These are overdamped, or *evanescent* modes⁴, that show pure decay without oscillation. Also, they are evenly spaced in the limit, and the smallest root approaches zero. In Appendix A, we show analytically that

$$\lim_{r_b \rightarrow 1} \omega_n = i\kappa n, \quad n = 0, 1, 2, 3 \dots, \quad (43)$$

where κ is the surface gravity (30). As r_b is increased, pairs of imaginary roots merge together and then move off on a trajectory with nonzero real part.

- Also in both cases, there is a tendency for the frequencies to fan out and then migrate towards the real axis as r_b is increased further, past the pure tension threshold.
- The two cases exhibit quite different behaviour in the far brane regime. For a small black hole ($\gamma = 20$), the roots move towards the real axis very quickly, ending up with $\text{Re}\omega_n$ much larger than $\text{Im}\omega_n$. This means that the several QNMs are lightly damped in this limit. On the other hand, the large black hole ($\gamma = 1/2$) has roots that drift more slowly towards the real axis, resulting in moderately damped modes. The exception is the fundamental, defined as the QNM with the smallest frequency, which becomes lightly damped in the

⁴ This is the common nomenclature in the theory of electromagnetic waveguides and other fields.

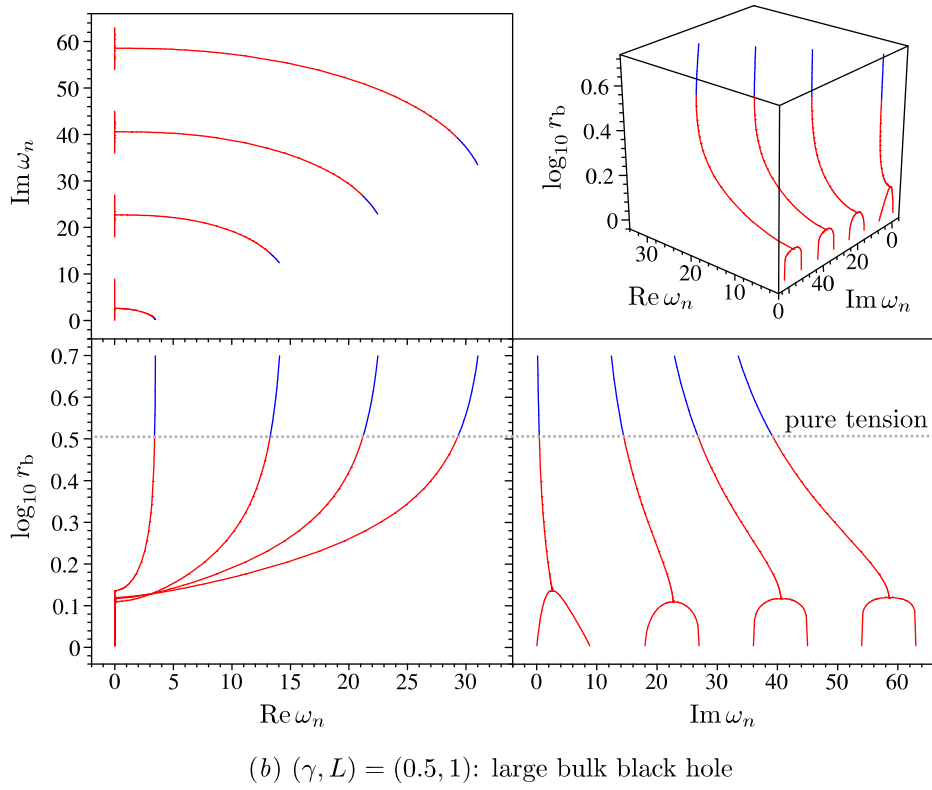
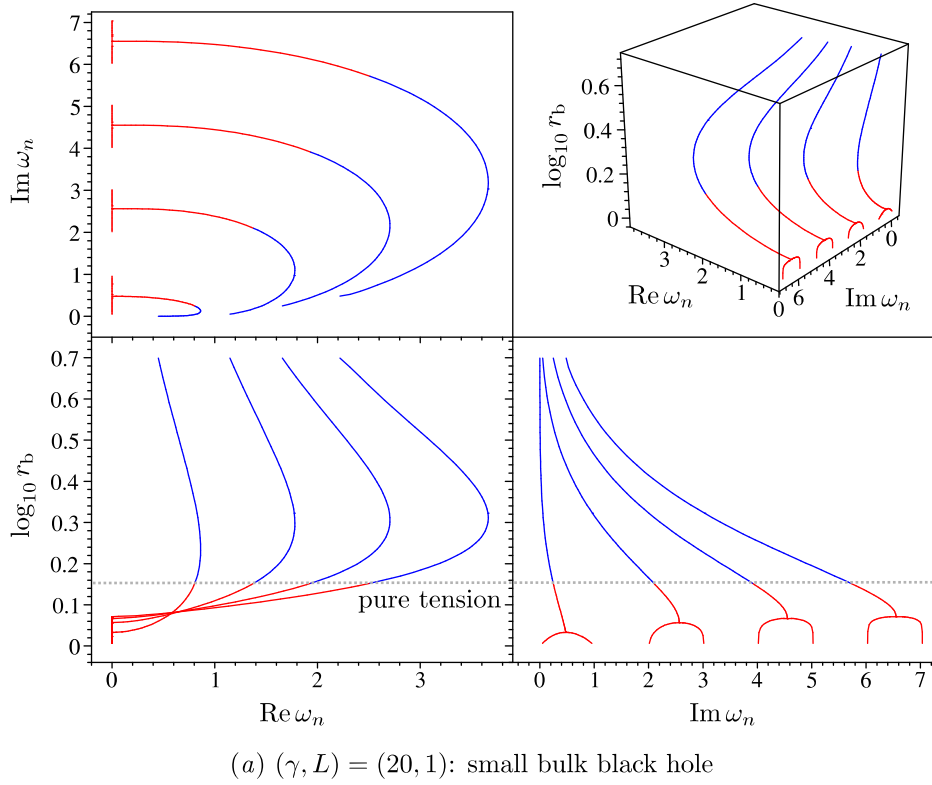


FIG. 4: QNM frequencies as a function of brane position; close brane roots are colored red, while far brane frequencies are blue

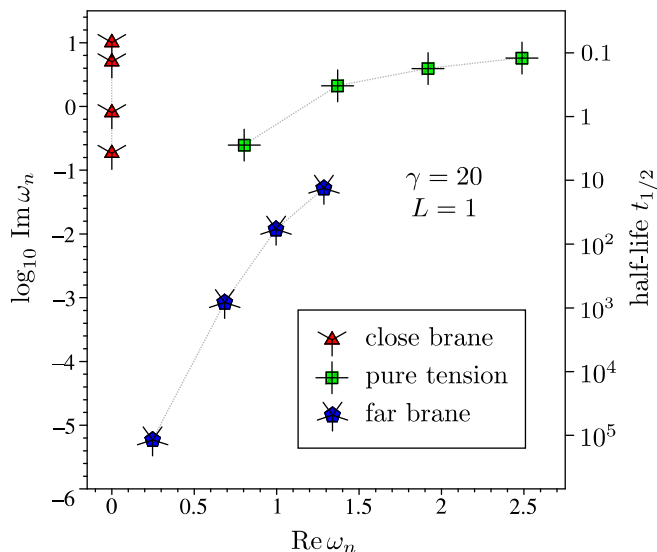


FIG. 5: QNM spectrum for close brane ($r_b = 1.05$), pure tension ($r_b = 1.42$), and far brane cases ($r_b = 10.00$) when $\gamma = 20$ and $L = 1$

far brane limit. Obviously, the reason for this discrepancy is that small black hole potential (Fig. 2) has a resonant cavity while the large black hole one (Fig. 3) does not.

The extreme close and far brane behaviour will be discussed in more detail in Secs. A and IV, respectively.

But first, let us consider the implications of the pattern of quasi-normal modes for actual gravity wave signals on the brane. To do this, we fix $\gamma = 20$ (i.e. a small black hole) and consider three separate brane positions corresponding to extreme close, pure tension, and extreme far brane positions. The four smallest QNMs for each case are shown in Fig. 5. We have plotted the imaginary parts of the modes on a logarithmic scale because the damping varies by orders of magnitude from case to case. The right axis shows the half-life, defined as the time it takes for the modes amplitude to decrease by a factor of 1/2. The principal difference between the close and pure tension cases is that the $\text{Re } \omega_n = 0$ in the former. The half-lives of the mode are similar, and less than about 10. However, the fundamental mode in the far brane case has $t_{1/2} \sim 10^5$, which is extremely long compared to the other cases. In fact, all of the far brane modes shown have very small imaginary parts compared to the other cases. This types of behaviour are consistent with the speculation of Sec. III A—the resonant cavity is an efficient gravity wave trap.

We now perform ‘numeric scattering experiments’ for each of the three cases shown in Fig. 5. These consist of numeric solutions of the PDE (21) subject to specified initial data. In Fig. 6, we show the results of such integrations at the position of the brane. The initial data for each of the three cases was identical Gaussian pulses

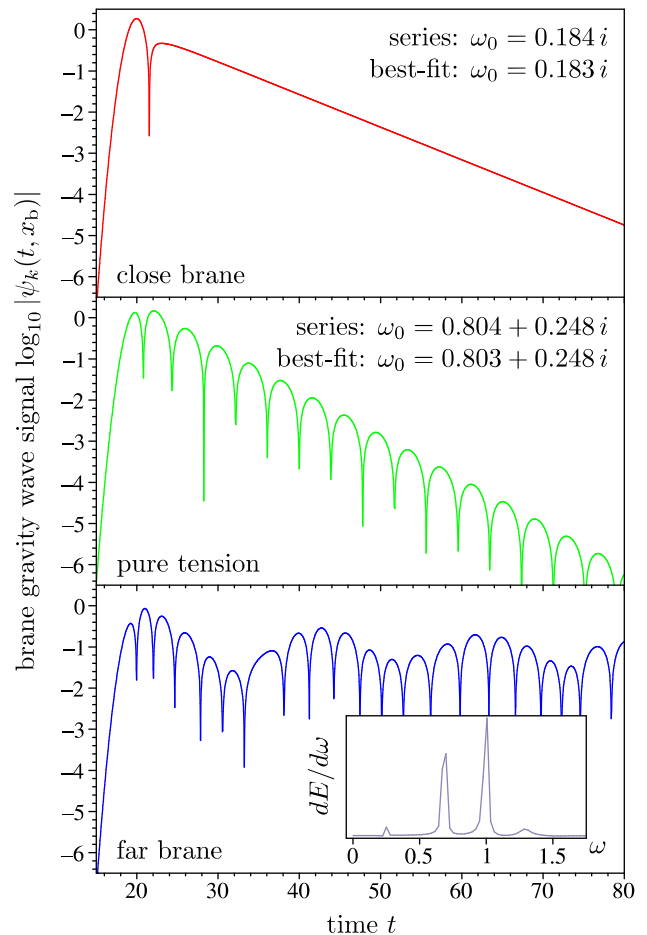


FIG. 6: Numeric brane gravity wave signals induced by a Gaussian pulse striking the brane when $(\gamma, L) = (20, 1)$ and $r_b = 1.05, 1.42, 10.00$ from top to bottom. In all cases, the incident pulse has a width of 2 and is centered about $x_0 = x_b - 20$ at $t = 0$. The ‘best-fit’ values of ω in the top two panels were found by matching a $\text{Re}(Ae^{i\omega t})$ template to the late-time signal, while the ‘series’ value comes from Sec. III C. The inset for the last case shows the Fourier transform of ψ_k between $t = 25$ and 250

incident on the brane at $t = 0$. The resulting signals reflect the characteristics of the QNM spectra seen in Fig. 5. The close brane waveform is a purely decaying exponential with no oscillations. On the other hand, the pure tension signal takes the form of a sinusoid with a collapsing envelope. In both of these cases, the fundamental mode’s lifetime is relatively large compared to the first overtone, so we see signals dominated by one quasi-normal frequency. We can thus fit $\text{Re}(Ae^{i\omega t})$ templates to the signal to numerically determine the fundamental frequency ω_0 . These are the ‘best-fit’ values shown in the upper two panels. Also shown are the frequencies determined from the series solution shown in Fig. 5, and the agreement between the two methods is excellent.

The far brane signal in the lower panel is markedly different. We see in Fig. 5 that three of the far brane

QNMs have lifetimes longer than the horizontal axis of Fig. 6, and the fourth's half-life is of the same order. So we expect contributions from all of the modes, which is exactly what is seen: a superposition of lightly damped QNMs. The signal is not adequately described by a single complex exponential, so we cannot find ω_0 by fitting. Instead, we plot the absolute square of the fast Fourier transform (FFT) of the signal between $t = 25$ and 250 in the inset. The power spectra is peaked at the real parts of the four QNMs, showing that all of them contribute to the signal. What is misleading about the Fourier transform, however, is the nature of the peaks. We shall discuss this in detail in the next Section, but for now let us note the following: The peaks are located at the QNM frequencies; the signal near these goes like $\exp(i(\varpi + i\Gamma/2)t)$, implying the power spectrum behaves like a Lorentzian, $\propto 1/[(\omega - \varpi)^2 + (\Gamma/2)^2]$. Thus we expect the widths of the peaks in Fig. 6 to be of order of the square of the imaginary part of the QNM: this is extremely narrow, and not easily resolvable numerically.

To summarize this section: We have found that when the brane is very close to the horizon, all the quasi-normal frequencies are purely imaginary. This makes the gravity wave signal a simple decaying exponential, as in the top panel of Fig. 6. For intermediate brane radii, the real and imaginary parts of the QNMs have roughly the same magnitude, resulting in a ‘classic’ ringdown signal; i.e., the monochromatic damped oscillations seen in the middle panel of Fig. 6. The far brane behaviour depends on the size of the bulk black hole. If it is large, the far brane behaviour is not much different than the pure tension regime. But if the black hole is small, the resonant cavity between the brane and the photon sphere allows for a number of lightly damped QNMs. This results in a long-lived multi-frequency brane signal, as seen in the bottom panel of Fig. 6.

IV. QUASI-BOUND STATES

As mentioned above, the main drawback of our series method of finding quasi-normal frequencies is that it becomes unfeasible as $r_b \rightarrow \infty$. This is indeed unfortunate, because as Fig. 6 demonstrates, some of the most interesting gravitational waveforms are associated with large brane radii. As seen in Figs. 4 and 5, this is due to QNMs with very small imaginary parts. We are naturally curious about the behaviour of these modes as r_b becomes larger and larger, which motivates us to find a different method of locating the system’s resonances when the imaginary part is small. Our techniques will be based on collision theory in ordinary quantum mechanics [27, 28] and numeric solution of the wave equation in the frequency domain. Most interesting effects are associated with the resonant cavity between the brane and the bulk potential peak, so we will mostly highlight the small black hole case in this section. In Sec. IV E, we indicate how the conclusions translate into the big black

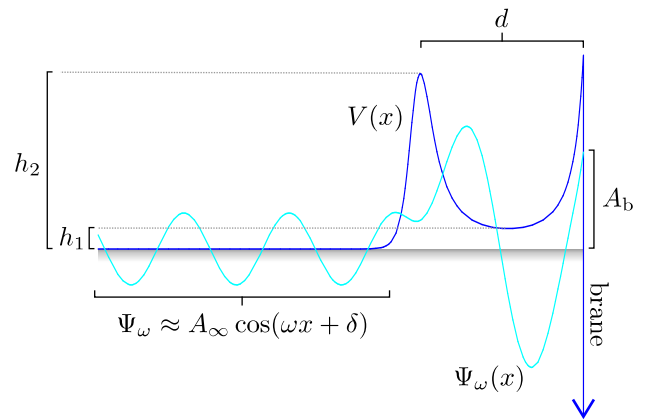


FIG. 7: Numeric solution of the master wave equation in the frequency domain for a far brane, small black hole scenario. The plot also shows the definitions of various quantities appearing in the main text

hole scenario.

A. The scattering matrix and the trapping coefficient

In the beginning of Sec. III A, we wrote $\psi_k = e^{i\omega t} \Psi_{k\omega}$ and hence transformed the master wave equation into a time-independent Schrödinger equation (28) with energy parameter $E = \omega^2$ and boundary condition (29). Here, we consider the (numeric) solutions of this ODE with ω real. As in Sec. III B, we will simplify our notation by dropping the wavenumber k label from all quantities.

In Fig. 7, we show the results of a typical integration for a far ES brane, small black hole, and a given value of ω . As could have been deduced from the potential, the solution Ψ_ω satisfying the brane boundary conditions takes the form of a simple sinusoid as $x \rightarrow -\infty$. We can write this asymptotic solution as

$$\Psi_\omega \approx \frac{1}{2} A_\infty e^{-i\delta} [e^{-i\omega x} + S(\omega) e^{i\omega x}], \quad (44)$$

where $S(\omega) = e^{2i\delta}$ is the so-called *scattering matrix* and $\delta = \delta(\omega)$ is the *scattering phase shift*.⁵ Presented in this way, Ψ_ω is an explicit superposition of right and left moving waves.

Now, we consider the continuation of S to complex values of ω . Suppose that the potential supports a QNM with $\text{Im } \omega_n \ll 1$. Then, we require that S have a pole at

⁵ In our case, the scattering ‘matrix’ is clearly a scalar quantity. This is because we are really looking at single-channel scattering, where there is no change of identity of the graviton as it scatters off the brane. Multi-channel scattering is common in nuclear physics, where the projectile and target can turn into different particles after the collision, which requires S to be matrix-valued.

$\omega = \omega_n$ in order to ensure that Ψ_ω is a purely outgoing solution. For simplicity, we assume that this is a simple pole. Also note that the scattering matrix is unitary $SS^* = 1$ when ω is real. Under these circumstances, the leading order Laurent expansion of S about its pole must be of the form [27]

$$S(\omega) \approx e^{2i\delta_{\text{bg}}} \frac{\omega - \omega_n^*}{\omega - \omega_n}, \quad (45)$$

where δ_{bg} is the ‘background’ phase shift, which is an unspecified, slowly varying real function of ω for our purposes. If we now write the n th QNM as

$$\omega_n = \varpi_n + \frac{1}{2}i\Gamma_n, \quad (46)$$

we see that the total phase shift, with ω real and near to ϖ_n , is of the form

$$\delta(\omega) \approx \delta_{\text{bg}}(\omega) - \arcsin \frac{\Gamma_n}{\sqrt{4(\omega - \varpi_n)^2 + \Gamma_n^2}}. \quad (47)$$

Because Γ_n is small, the second ‘resonant’ contribution implies that $\delta(\omega)$ will vary rapidly about $\omega = \varpi_n$. Indeed, we expect that the phase will change by π as ω is varied across the resonance. The traditional way of identifying a resonance is to calculate $\delta(\omega)$ for a given potential and look for sharp features in $\sin^2 \delta(\omega)$.⁶ Such lines will be centered about $\omega = \varpi_n$ and have widths proportional to Γ_n , which means that long-lived QNMs give rise to narrow features.

But is there a more physical quantity than $\sin^2 \delta(\omega)$ to examine? Recall that QNMs are supposed to be metastable bound states, so we intuitively expect that Ψ_ω to be localized near the brane for $\omega \approx \varpi_n$. We can quantify this expectation by defining the *trapping coefficient*:

$$\eta(\omega) = \frac{A_b}{A_\infty}, \quad (48)$$

where A_b is the magnitude of Ψ_ω on the brane (see Fig. 7). Any state with $\eta(\omega) \gg 1$ will correspond to the graviton being more localized near the brane than at infinity; this will be a ‘quasi-bound’ state. In fact, *if* our potential supported a stable bound state with $\text{Im} \omega_n = 0$, we would have $\eta(\omega_n) = \infty$.

Quantitatively, more can be said about $\eta(\omega)$ near resonance by writing

$$\Psi_\omega(x) = \text{Re} [e^{i\delta} \Psi_\omega^{(\text{out})}(x)], \quad (49)$$

where $\Psi_\omega^{(\text{out})}(x)$ is the purely outgoing solution

$$\Psi_\omega^{(\text{out})}(x) = \begin{cases} e^{i\omega x}, & x = -\infty, \\ R e^{i\theta}, & x = x_b. \end{cases} \quad (50)$$

Here, R and θ are assumed to be slowly-varying real functions of ω . This gives

$$\xi(\omega) = \eta^2(\omega) = R^2(\omega) \sin^2[\delta(\omega) + \theta(\omega) - \pi/2]. \quad (51)$$

Now, suppose that the phases satisfy

$$\delta_{\text{bg}}(\omega) + \theta(\omega) \approx \pi/2 \text{ or } 3\pi/2, \quad \text{for } \omega \approx \varpi_n, \quad (52)$$

then we have

$$\xi(\omega) \approx R^2(\omega) \frac{\Gamma_n^2}{4(\omega - \varpi_n)^2 + \Gamma_n^2}, \quad \text{for } \omega \approx \varpi_n. \quad (53)$$

Under this assumption, we expect ξ_{res} to be peaked about the real part of each lightly damped QNM. Furthermore, the shape of the peak is Lorentzian (or Breit-Wigner) with a half-width at half-maximum equal to the imaginary part of the mode. Of course, if $\delta_{\text{bg}} + \theta$ is not approximately $\pi/2$ or $3\pi/2$ there is still a resonant feature, but with a more complicated lineshape.

The only way to constrain these ‘nuisance’ phases is via direct calculation. In Fig. 8, we plot $\xi(\omega)$ for the $(\gamma, r_b, L) = (20, 10, 1)$ case. The spectrum features a number of discrete peaks, and the positions of the first few peaks match the real parts of the QNM frequencies calculated in Sec. III C for this case. We can make this more precise by subtracting a smooth baseline from $\xi(\omega)$ to remove some of the non-resonant part of the spectrum; i.e., contributions from the variations of δ_{bg} and θ with ω . The insets of Fig. 8 show magnifications of the baseline-subtracted spectrum about the expected positions of the first three QNMs from the series solution; and the frequency range of each inset has been set to be 20 times the imaginary part. The shapes of the three lines are virtually identical and extremely well approximated by the Lorentzian template (53). Hence, this example suggests that it is reasonable to take $\delta_{\text{bg}} + \theta \approx \pi/2$ or $3\pi/2$ near an ES quasi-normal resonance. Furthermore, we see that the *height* of the peaks gives us roughly $R(\omega)^2$, after the baseline is subtracted. We have actually calculated the spectral function $\xi(\omega)$ for many other cases, and found that the first few peaks in ξ always have a Lorentzian profile.

So, we have a straightforward algorithm for *estimating* lightly damped quasi-normal frequencies: First, find $\xi(\omega)$ from the numeric solution of the ODE (28). Then, subtract a baseline and find all of the features in ξ_{res} with a Lorentzian profile. The real and imaginary parts of the frequencies are simply related to the position and width of the those peaks. We will call resonances identified in this fashion *quasi-bound states* (QBSs) for two reasons: First, since they maximize the trapping coefficient they are, in some sense, brane-localized modes with $A_b \gg A_\infty$. Second, they all have $\text{Im} \omega_n \ll 1$; i.e., they are extremely long-lived excitations. Of course, QBSs are merely a sub-class of QNMs, but we will see below that they dominate the phenomenology for far branes.

Finally, we should stress that this trapping coefficient method really just estimates the QBS frequencies. This is

⁶ Algorithms very similar to this (so-called ‘resonance’ methods) have been used to identify lightly-damped QNMs of neutron stars [29, 30].

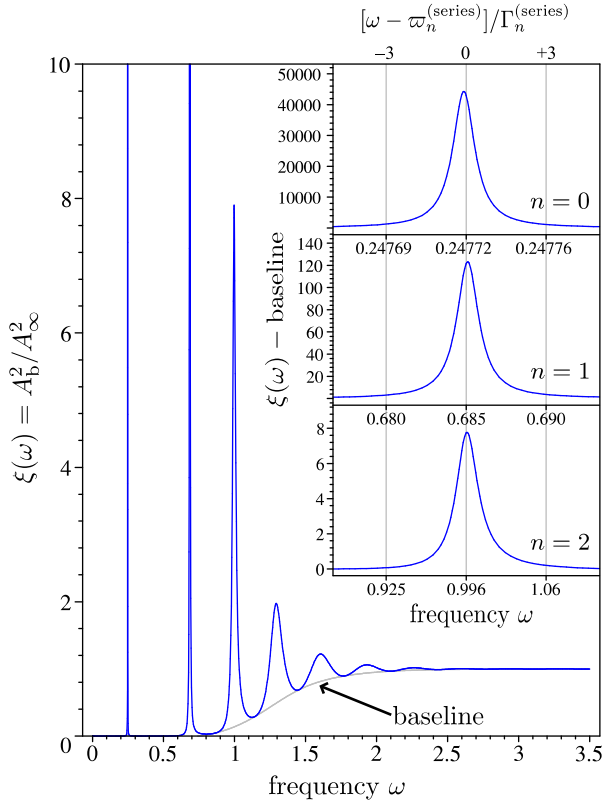


FIG. 8: The square of the trapping coefficient $\xi(\omega) = \eta^2(\omega)$ in the $(\gamma, r_b, L) = (20, 10, 1)$ case. The insets show the magnified views of the spectrum with a smooth baseline—shown in the main figure—subtracted. As described in the text, we expect the baseline-subtracted peaks to have a Lorentzian lineshape (53) with ϖ_n and Γ_n given by the series solution of Sec. III C. We define the root-mean-square discrepancy between the normalized peaks shown above ξ_t and the series prediction ξ_s , assuming a perfect Lorentzian, as $\epsilon = [\int (\xi_t - \xi_s)^2 d\omega]^{1/2} / \int \xi_s d\omega$. This leads to $\epsilon = 0.011, 0.0073, \text{ and } 0.0072$, respectively, which are very small discrepancies indeed

because the procedure is prone to several uncertainties; including the non-uniqueness of our choice of baseline, deviations from Lorentzian profiles due to the running of δ_{bg}, R and θ with ω , the validity of the Laurent expansion (45), etc. However, having said that, we find remarkable agreement between this ‘trapping coefficient’ method and the series solution in the $(\gamma, r_b, L) = (20, 10, 1)$ case:

$$\omega_0 = \begin{cases} 0.247721 + 5.90 \times 10^{-6} i & (\text{series}) \\ 0.247720 + 5.88 \times 10^{-6} i & (\text{trapping}) \end{cases},$$

$$\omega_1 = \begin{cases} 0.6852 + 8.45 \times 10^{-4} i & (\text{series}) \\ 0.6853 + 8.51 \times 10^{-4} i & (\text{trapping}) \end{cases}.$$

Such accuracy is more than sufficient for our purposes, so we now proceed to use the ‘trapping method’ to calculate the QBS frequencies that the series solution has difficulties with.

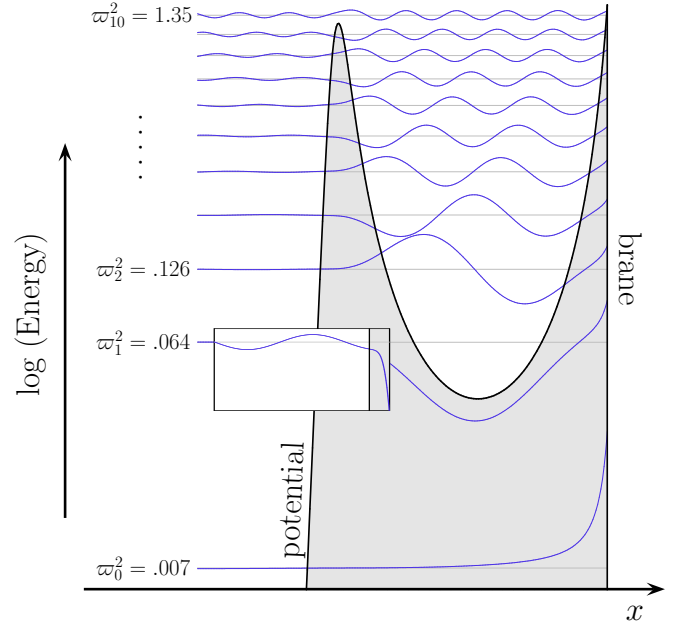


FIG. 9: Spatial wavefunctions $\Psi^n(x)$ of the first 11 quasi-bound states in the $(\gamma, r_b, L) = (20, 250, 1)$ case.

B. Resonant cavity quasi-bound state wavefunctions

Much intuition about the QBS solutions can be gained by examining their spatial profiles $\Psi^n(x) = \Psi_{\varpi_n}(x)$. We plot these spatial profiles in Fig. 9 for the $(\gamma, r_b, L) = (20, 250, 1)$ case. The mode with the smallest frequencies is labelled with $n = 0$ and is the fundamental, while the other modes are the ‘overtones’. The logarithm of the potential $V(x)$ is shown in the background. The vertical offset of each Ψ^n corresponds to the energy parameter $E_n = \varpi_n^2$ defining the solution. We see that the overtone energies are greater than the potential within the resonant cavity, while the fundamental’s energy only becomes greater than V in the asymptotic region. (Referring to Fig. 7, this can be expressed as $\varpi_0^2 < h_1$, while $\varpi_n^2 > h_1$ for $n = 1, 2, \dots$) As in ordinary quantum mechanics, the wavefunctions have concave curvature ($\Psi''/\Psi < 0$) when their energy is greater than the potential, and convex curvature ($\Psi''/\Psi > 0$) otherwise. Hence, the overtone profiles oscillate in the resonant cavity while the fundamental shows monotonic decay.

The integer n actually counts the number of nodes—places where the wavefunction crosses zero between the brane and the peak in V . This is also the number of local extrema—or ‘loops’—in the wavefunction in this region. That is, Ψ^1 has one minima in the resonant cavity, Ψ^2 has one minima and one maxima, etc. And the fundamental has none. This type of behaviour is strongly reminiscent of energy eigenfunctions in quantum mechanics, as in the radial eigenfunctions of the hydrogen atom, for example.

The distribution of energies causes the $n = 0$ mode to be the only wavefunction sharply localized near the

brane. Conversely, the overtone wavefunctions are dispersed throughout the resonant cavity (and beyond for high-energy modes). This type of behaviour generalizes to all of the other cases we have looked at.

The key point here is that the ‘quasi-bound state’ moniker is well deserved for the lowest-lying modes, whose amplitude at infinity A_∞ is vanishingly small. The inset shows a magnified view of the $n = 1$ wavefunction in the asymptotic region to emphasize that it is actually sinusoidal and nonzero. The shape of the overtone wavefunctions suggests a tunnelling process where ‘most’ of the graviton is confined to the right of the barrier, but a small portion leaks through to infinity. This leakage is more pronounced for higher energy modes, corresponding to larger imaginary parts – so wider Lorentzian profiles – for these frequencies.

Now that we have a fuller understanding of the trapping method and the quasi-bound states which it finds, we turn to a deeper investigation of the three dimensional parameter space of the model. We shall look at varying r_b , L , and γ in turn.

C. Far brane limit: recovering the zero-mode and evenly-spaced overtones

The trapping method allows us to further investigate the trends in the QNM frequencies shown in Fig. 4 to larger values of r_b in the small black hole case (γ large). In Fig. 10, we show the real and imaginary parts of the quasi-normal frequencies when $(\gamma, L) = (20, 1)$ as a function of r_b . The most striking feature of this plot is the disparate behaviour of the fundamental and overtone modes. While the imaginary parts of the overtones approach constant values as $r_b \rightarrow \infty$, $\text{Im} \omega_0$ decays to zero as a power law. Hence, for infinitely large branes, we recover a single stable graviton mode confined to the brane.

But is this infinite lifetime excitation the ES generalization of the RS zero-mode? In 4 dimensions, tensor perturbations of an Einstein static universe would oscillate with frequency $\sqrt{L(L+2)}/r_b$ according to comoving observers [25]. Taking into account the redshift factor between the bulk coordinates and a comoving brane observer, this translates into a bulk frequency

$$\omega_{\text{GR}}(\gamma, r_b) = \frac{\sqrt{f_b L(L+2)}}{r_b}. \quad (54)$$

In Fig. 11, we plot the fundamental QBS frequency for a range of (γ, r_b) parameters. Also shown as horizontal lines in the top panel is the GR frequency in the $r_b \rightarrow \infty$ limit. We see very clearly that for all γ , ω_0 approached ω_{GR} asymptotically. Hence, not only do we have a mode with infinite lifetime in the large brane limit, the frequency of this mode matches what one might expect from ordinary 4-dimensional theory. These are the essential characteristics of the standard zero-mode in the

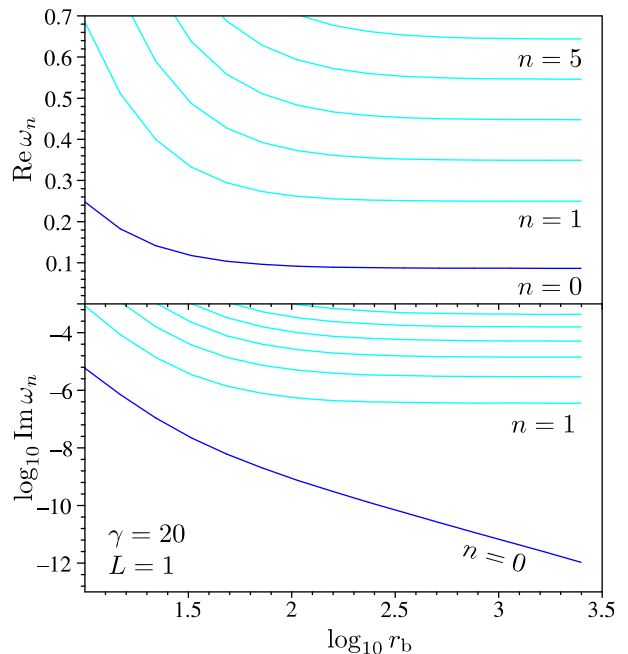


FIG. 10: Quasi-bound state frequencies as a function of brane position. Note that the fundamental frequency ω_0 tends to a real value as $r_b \rightarrow \infty$, while the imaginary parts of the overtone frequencies are asymptotically constant and non-zero.

RS scenario, so we conclude that as $r_b \rightarrow \infty$ we recover the zero-mode in the ES model.

This is a very sensible result. We saw above that the $n = 0$ wavefunction is distinguished from the others in several important ways, including being the only mode to be truly localized on the brane and nowhere else. So it is not surprising to find that its frequency shows a different dependence on r_b . Furthermore, in Ref. [3] we argued that the very existence of the bulk black hole was responsible for the delocalization of the zero-mode in the ES scenario. Here, we see that as the effects of the black hole at the brane position get smaller and smaller as r_b is increased, we ‘re-localize’ brane gravity. In other words, the gravitational field of the bulk black hole strips the zero-mode off the brane, but when the brane is far away this delocalization becomes more and more inefficient.

Some of the features seen in Figs. 10 and 11 can be understood using WKB-approximation techniques. In quantum mechanics, decay constants for metastable bound states can be approximated by the WKB tunnelling amplitude across the potential barrier responsible confining the wavefunction. The classic example of this kind of calculation is Gamov’s description of alpha-decay using elementary wave mechanics. As seen in Fig. 9, the energy of the fundamental mode lies beneath the resonant cavity; i.e., $\varpi_0^2 < h_1$. Hence, we can view its decay as a tunnelling process from the delta-function at the

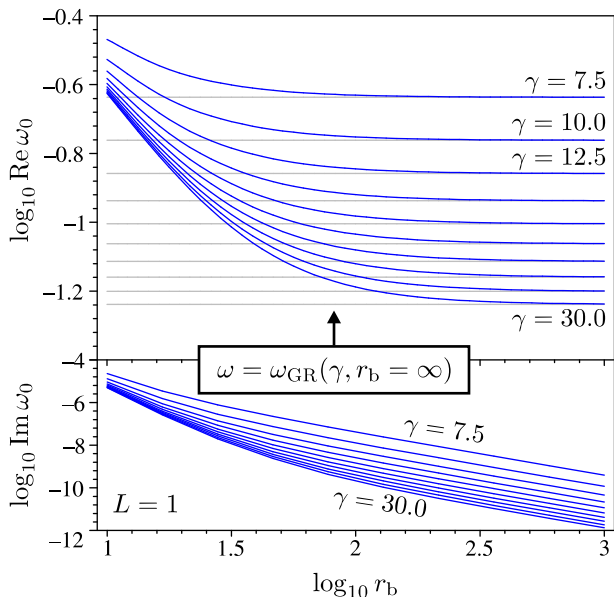


FIG. 11: Frequency of the fundamental QBS for varying γ and r_b . The horizontal lines in the top panel indicate the GR prediction for the frequency of tensor perturbations in an ES universe as $r_b \rightarrow \infty$. Clearly, ω_0 approaches ω_{GR} in the limit, suggesting that we recover a RS-like zero-mode for infinitely large branes.

brane position. This gives rise to

$$\text{Im } \omega_0 \sim \exp \left[- \int_{x_0}^{x_b} \sqrt{V(x) - \varpi_0^2} dx \right]. \quad (55)$$

Here, x_0 is the ‘classical’ turning-point such that $\varpi_0^2 = V(x_0)$. Recall from Figs. 1 and 3 that the potential diverges at spatial infinity. This implies that as $r_b \rightarrow \infty$, the rightmost portion of the integrand diverges like $(x_\infty - x_b)^{-1}$, which in turn gives $\text{Im } \omega_0 \rightarrow 0$. Furthermore, it is not difficult to show that

$$\text{Im } \omega_0 \propto r_b^{-\sqrt{15}/2}, \quad \text{as } r_b \rightarrow \infty. \quad (56)$$

This is exactly the asymptotic behaviour seen in Fig. 11: $\log_{10} \text{Im } \omega_0$ versus $\log_{10} r_b$ is a straight line for large brane radii whose slope is independent of γ . We expect this behaviour to generalize to other choices of L .

Turning our attention to the overtone modes, we note that their energies satisfy $h_1 < \varpi_n^2 < h_2$, so there are three turning points $x_0 < x_1 < x_2$. The potential barrier that is responsible for the quasi-confinement is the peak in $V(x)$ shown in Fig. 9. This peak does not become infinitely large in the limit, which explains why the overtones have finite damping asymptotically. In this case, WKB techniques can tell us something about the real parts of the QBS frequencies. Because the overtone energies are greater than the potential inside the resonant cavity, we can use the Bohr-Sommerfeld quantization rule

[28] to write:

$$\int_{x_1}^{x_2} dx \sqrt{\varpi_n^2 - V(x)} = (n + \frac{1}{2})\pi, \quad n \geq 1. \quad (57)$$

If we approximate the potential in the cavity by its average value, we obtain:

$$\begin{aligned} \varpi_n &\approx \sqrt{\bar{V} + \left[\frac{(n + \frac{1}{2})\pi}{\Delta x} \right]^2} \\ &\rightarrow \frac{(n + \frac{1}{2})\pi}{\Delta x} \quad \text{for } \bar{V} \ll \frac{n^2}{(\Delta x)^2}, \end{aligned} \quad (58)$$

where $\Delta x = x_2 - x_1$. The last approximation holds reasonably well for the higher modes in the current problem. Finally, as $r_b \rightarrow \infty$ we have $\Delta x \approx d$, where d is the distance between the brane and the potential peak (cf. Fig. 7). In the limit d becomes constant, which explains why $\text{Re } \omega_n$ becomes asymptotically constant and evenly spaced for the overtones in Fig. 10.

D. Small scale limit: the quasi-bound states become bound

So far we have concentrated on perturbations with $L = 1$; now consider perturbations with L not necessarily equal to unity. The value of L controls the wavelength of the gravity waves tangent to the brane, so when we increase L we are examining smaller and smaller scales. What kind of modes will exist in this case?

In Fig. 12, we plot the logarithm of the trapping coefficient $\xi(\omega)$ for the $(\gamma, r_b) = (20, 250)$ case, but now letting L increase from 1 through 5 to 10. The principle effect of increasing L is to increase the number and sharpness of the spikes – implying more quasi-bound states with much lighter damping. The WKB approximation can again be used to understand this behaviour.

Returning to (55), we take the $L \rightarrow \infty$ limit instead of $r_b \rightarrow \infty$. The height of the peak in the potential scales like

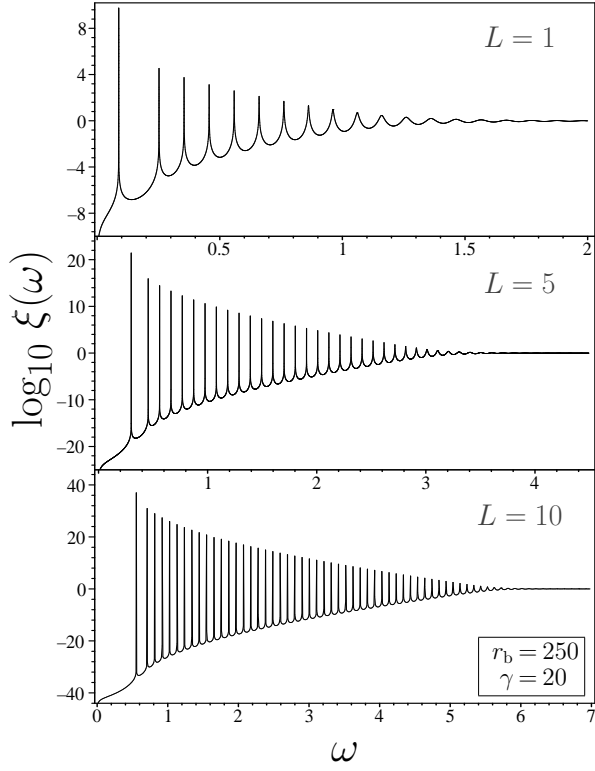
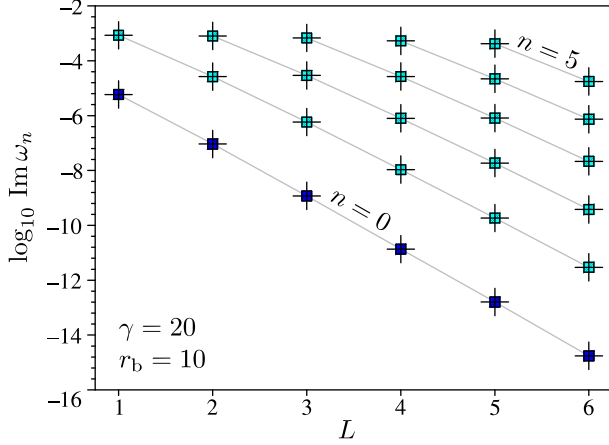
$$h_2 \approx \frac{(\gamma^2 + 2)^2}{4\gamma^2(\gamma^2 + 1)} L^2, \quad (59)$$

so its contribution dominates the integral. The same holds if we apply the formula to the overtones by switching ϖ_0 to ϖ_n and x_b to x_1 . In any case, this leads to

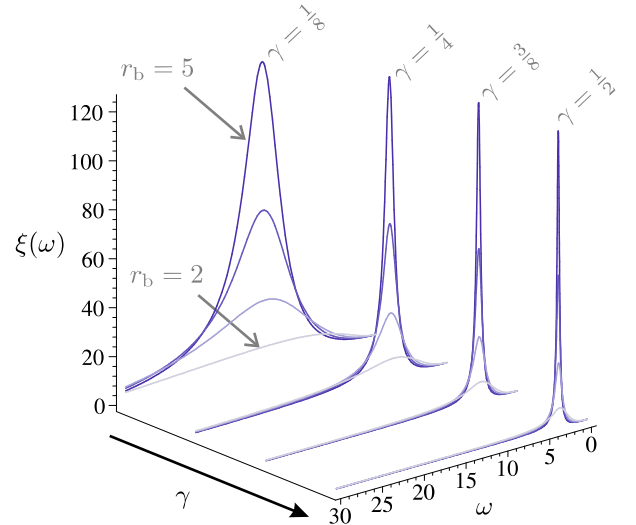
$$\text{Im } \omega_n \propto e^{-aL}, \quad \text{as } L \rightarrow \infty, \quad (60)$$

where a is a constant depending on γ and r_b . This exponential decay in the widths of the spikes is shown in Fig. 13, where we plot the imaginary parts of the QBS frequencies for various scales.

Physically, this is intriguing: As the spatial scale of perturbations on the brane decreases, their bulk angular momentum around the black hole increases. This

FIG. 12: Variation of the trapping coefficient with L .FIG. 13: The variation of the imaginary parts of QBS frequencies with L .

causes the centrifugal barrier between the brane and the event horizon to grow taller and taller, which in turn makes it difficult for gravity waves to tunnel away from the brane into the black hole. The net result is that the confinement of the QBSs in the resonant cavity becomes 100% efficient. Effectively, the quasi-normal modes become normal modes when their imaginary parts disappear; the quasi-bound states become bound when A_∞ goes to zero. This is like a two-brane model where the potential barrier takes the role of the shadow brane. We will discuss the implications for cosmology below.

FIG. 14: $\xi(\omega)$ for various $L = 1$ big black hole scenarios

How many QBS states are there in the large L limit? Above we saw that high overtones have $\omega_n \sim \pi(n + \frac{1}{2})/d$. The highest QBS mode should have an energy comparable to the height of the potential peak; i.e., $\omega_N^2 \sim h_2$. Finally, we know that the height of the peak scales as $L(L + 2)$, which yields that the number of quasi-bound states is proportional to L as $L \rightarrow \infty$.

E. The big black hole case

To this point, we have only applied the trapping coefficient method to small black hole cases featuring a resonant cavity. But under certain circumstances, we can also use the procedure when γ is small.

The square of the trapping coefficient for range of relatively small values of γ and r_b are shown in Fig. 14. All the spectra show one peak indicating the existence of only one QBS solution. This is because there is no resonant cavity when γ is small (see Fig. 3), hence there are no overtones. The general trend is for the peak position to show little variation with r_b , and to decrease with increasing γ . On the other hand, the width of the feature decreases as either γ or r_b is increased.

The rather broad nature of the peaks for small (γ, r_b) means that they are not well approximated by Lorentzian profiles, which suggests no modes with tiny imaginary parts. This is consistent with the series results of Sec. III C, where small imaginary parts were only achieved for large brane radii. When r_b is large, the fundamental-mode WKB analysis of Sec. IV C is applicable to this case, implying that the imaginary part of the sole QBS frequency goes to zero for large branes. We have confirmed this numerically, and also confirmed that the real parts approach ω_{GR} . So, we also recover the GR zero-mode as $r_b \rightarrow \infty$ in the big black hole case.

As in the small black hole case, the potential barrier

between the brane and the horizon scales as $L(L+2)$ for large L . Hence, the conversion of quasi-bound into bound states as $L \rightarrow \infty$ also occurs for small γ , the chief difference being that there is only the fundamental mode to convert.

The main difference between the small and large black hole cases, then, is that in the former there are quasi-bound state overtones, while in the latter there are not. However, there is always a fundamental $n=0$ QBS, and the limiting behaviour of that mode as r_b or L becomes large is the same irrespective of γ .

V. THE INITIAL VALUE PROBLEM

In Sec. III C, we solved the wave equation in the time domain to illustrate the effects of the QNMs on actual brane signals. Here, we examine this problem in more detail by considering several different classes of initial data. We will demonstrate that the trapping coefficient η is useful for more than just finding QBSs; it actually plays a prominent role in determining the power spectrum of the brane signal. We also consider the scattering of wave packets in scenarios featuring a resonant cavity, and observe coherent ‘bouncing’ behaviour. Finally, we allow for ‘initial data’ representing the situation where the brane is in thermal equilibrium with the semi-classical Hawking flux from the black hole.

A. Green’s function analysis

Suppose that at $t=0$, we specify the both the value and first time derivative of ψ . Then, we can construct a formal Green’s function solution for the signal on the brane $\psi_b(t) = \psi(t, r_b)$ by following the standard technique from black hole perturbation theory [1, 31]. This involves applying the Laplace transform to the master wave equation to convert the initial data into a source term, obtaining the Green’s function solution, and then performing the reverse transform to return to the time domain. If we write the resulting solution as an integral in Fourier space, we obtain

$$\psi(t, x) = \frac{1}{2\pi} \int d\omega dx' e^{i\omega t} G_\omega(x, x') \mathcal{I}(x', \omega), \quad t > 0. \quad (61)$$

Here,

$$\mathcal{I}(x', \omega) = -i\omega\psi(0, x') - \dot{\psi}(0, x'). \quad (62)$$

As usual, the Green’s function is composed of solutions to the frequency domain homogeneous equation (28):

$$G_\omega(x, x') = \frac{\Psi_\omega^{(L)}(x_{<})\Psi_\omega^{(R)}(x_{>})}{W[\Psi_\omega^{(L)}, \Psi_\omega^{(R)}]}, \quad (63)$$

where $\Psi_\omega^{(L)}$ is the ODE solution that satisfies the outgoing boundary condition at $x = -\infty$, $\Psi_\omega^{(R)}$ satisfies

the boundary condition at the brane, $x_{<} = \min(x, x')$, $x_{>} = \max(x, x')$, and $W = \Psi_\omega^{(L)}\Psi_\omega^{(R)'} - \Psi_\omega^{(L)'}\Psi_\omega^{(R)}$ is the Wronskian. In this section, it is useful to choose the x -coordinate such that $x_b = 0$. Using the definitions and results of Sec. IV A, we have

$$\Psi_\omega^{(L)}(x) = \begin{cases} e^{i\omega x}, & x \rightarrow -\infty, \\ Re^{i\theta}, & x = x_b \equiv 0, \end{cases} \quad (64a)$$

$$\Psi_\omega^{(R)}(x) = \begin{cases} \cos(\omega x + \delta), & x \rightarrow -\infty, \\ \eta(\omega), & x = x_b \equiv 0. \end{cases} \quad (64b)$$

Because there is no linear derivative in the Schrödinger equation (28), the Wronskian is independent of x and we can evaluate it at $x = -\infty$

$$W[\Psi_\omega^{(L)}, \Psi_\omega^{(R)}] = -i\omega e^{-i\delta}. \quad (65)$$

If we now select the field point to lie on the brane $r = r_b$, our solution for ψ reads

$$\psi_b(t) = \int d\omega e^{i\omega t} e^{i\delta} \eta(\omega) \hat{\mathcal{I}}(\omega), \quad t > 0, \quad (66)$$

where

$$\hat{\mathcal{I}}(\omega) = \frac{1}{2\pi} \int dx \Psi_\omega^{(L)}(x) \left[\psi(0, x) + \frac{1}{i\omega} \dot{\psi}(0, x) \right]. \quad (67)$$

Note the prominent role played by both the scattering matrix $S^{1/2} = e^{i\delta}$ and the trapping coefficient η in (66). There are two ways one can evaluate the ω integral: either by direct or contour integration. In the former, η appears directly in the Fourier transform of the brane signal. Since η is sharply peaked near QBS resonances, the frequency profile of the brane signal will be similarly peaked. On the other hand, if one does the integral by completing the contour in the upper-half plane, the poles in the scattering matrix will give the dominant contributions to the signal; and of those contributions, the QBS poles will be the longest-lived and hence most important. Hence, either method yields the same result.

There are two special cases worth highlighting. The first concerns the ‘scattering experiments’ where the initial data is a coherent compact pulse incident on the brane from the asymptotic region. We have $\psi(t, x) = f(t-x)$ before scattering, which allows us to swap ∂_t for $-\partial_x$ in (67). We can also approximate $\Psi_\omega^{(L)}(x) \approx e^{i\omega x}$. Integrating by parts gives

$$\hat{\mathcal{I}}(\omega) = \frac{1}{\pi} \int dx e^{i\omega x} \psi(0, x). \quad (68)$$

Hence, $\hat{\mathcal{I}}$ is the spatial Fourier transform of the initial data and $|\hat{\mathcal{I}}|^2$ the initial power spectrum. We can use this to construct the Fourier transform of the brane signal,

keeping in mind that $\psi_b(t < 0) = 0$ for this initial data:

$$\begin{aligned} Z_b(\omega') &= \int_{-\infty}^{\infty} dt e^{-i\omega' t} \psi_b(t) = \int_0^{\infty} dt e^{-i\omega' t} \psi_b(t) \\ &= \int_{-\infty}^{\infty} d\omega \left[\pi \delta(\omega - \omega') + \frac{i}{\omega - \omega'} \right] e^{i\delta} \eta(\omega) \hat{\mathcal{I}}(\omega). \end{aligned}$$

To go from the first to second lines, we have used the Fourier transform of the Heaviside function. The integral associated with the first term in square brackets is trivial. The second integral expands as:

$$\frac{i}{\pi} \int_{-\infty}^0 dx \psi(0, x) \int_{-\infty}^{\infty} d\omega \frac{e^{i\omega x} e^{i\delta} \eta(\omega)}{\omega - \omega'}.$$

The pole at $\omega = \omega'$ means that we must evaluate this as a principal value integral. Since $x < 0$, we complete the contour in the lower half plane where the scattering matrix is analytic (η is analytic everywhere). Assuming the integral over the semi-circle at infinity vanishes, we obtain

$$Z_b(\omega) = 2\pi e^{i\delta} \eta(\omega) \hat{\mathcal{I}}(\omega), \quad \frac{dE}{d\omega} = 4\pi^2 \xi(\omega) |\hat{\mathcal{I}}(\omega)|^2, \quad (69)$$

where we have defined the power spectrum in the usual way $dE/d\omega = |Z_b(\omega)|^2$. Physically, this says that the gravity wave power seen on the brane is given by the power in the initial pulse times $\xi(\omega)$. In this sense, one could call $\xi(\omega)$ a ‘filter-factor’, in that it tells us how the potential processes an input from infinity into a brane signal. Of course, influence of the QBSs is dominant in this process, because they give rise to the dominant features in $\xi(\omega)$.

The second special case concerns brane localized initial data:

$$\begin{aligned} \psi(0, x) &= A \delta(x), \quad \dot{\psi}(0, x) = B \delta(x), \\ \hat{\mathcal{I}}(\omega) &= \frac{R e^{i\theta}}{2\pi} \left(A + \frac{B}{i\omega} \right). \end{aligned} \quad (70)$$

A similar argument to before gives the power spectrum

$$\frac{dE}{d\omega} = \xi(\omega) R^2(\omega) \left[A^2 + \frac{B^2}{\omega^2} \right]. \quad (71)$$

This is a little more complicated than the scattering experiment case (69) in that knowledge of the trapping coefficient and initial data is not enough to determine $dE/d\omega$, one also needs to know $R(\omega)$. But we do know the behaviour near QBS resonances

$$\frac{dE}{d\omega} \approx \left[A^2 + \frac{B^2}{\omega^2} \right] \frac{R^4(\omega) \Gamma_n^2}{4(\omega - \varpi_n)^2 + \Gamma_n^2}, \quad \omega \approx \varpi_n. \quad (72)$$

Hence, the system’s resonances manifest themselves as Lorentzian peaks in the power spectrum.

To summarize: In this section we have constructed the formal Green’s function solution for the brane signal. Both the scattering matrix and trapping coefficient appear explicitly in this solution, implying that the signal will be dominated by QBS resonances. The brane power spectra arising from the scattering of compact pulses from infinity is completely described by the pulses’ Fourier transform and ξ . However, more information is required for different types of initial data, including the brane-localized case. Regardless of the details, the prominence of η within the Green’s function ensures that $dE/d\omega$ is peaked about the ES resonant frequencies for any type of initial data.

B. Coherent states

Knowledge of the power in a given signal is not enough to reconstruct the signal in the time domain; much information is contained within the phase. So despite our understanding of the Green’s function of the problem, it is still useful to conduct numeric scattering experiments to see what kind of behaviour is possible.

In quantum potential problems featuring discrete wavefunctions, one can often construct ‘coherent state’ solutions that are wave packets whose dynamics mimic that of a classical particle travelling in the same potential. In the current problem, we know that far brane configurations have a number of lightly damped QBS modes. For example, the $(\gamma, r_b, L) = (20, 250, 1)$ case has around seven modes with lifetimes $t_{1/2} \gtrsim 1000$. On shorter timescales, these act like discrete bound states. Hence we can construct wave packets that behave like classical particles; for example, they can bounce back and forth within the resonant cavity. Of course, as time passes the QBS modes decay resulting in the decoherence of the pulse.

To see these effects explicitly, we consider a scattering process in the $(\gamma, r_b, L) = (20, 250, 1)$ case. The results of our numeric integration for ψ are shown in Fig. 15. Cosine modulated Gaussian initial data is fired at the potential barrier from well inside the photon sphere: a good percentage of this is reflected back to the black hole, while the transmitted part has had a redistribution of the frequencies which make it up, with preferential selection going to the frequencies corresponding to maxima of the trapping coefficient η . After scattering off the brane, the lowest frequencies in the signal become effectively trapped between the brane and the barrier, and bounce between them. While some leakage occurs at each bounce off the barrier, they cannot penetrate the barrier far, which means that they persist for a significant number of bounces. If we were to increase L in this experiment, we would see the bouncing last more or less indefinitely since the leakage at each bounce is so tiny.

To a brane observer things can look pretty strange. If the initial pulse is particularly narrow, the bouncing of the signal between brane and barrier would result in a

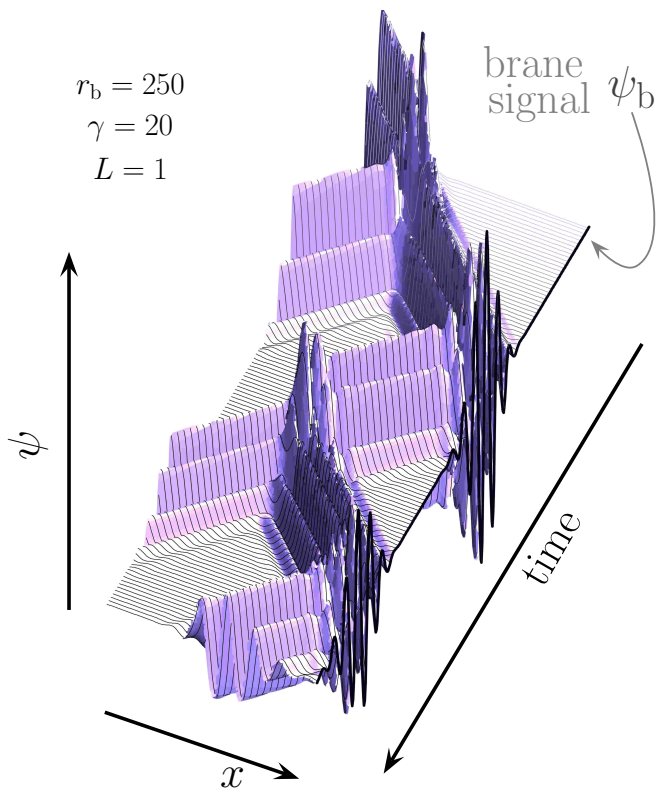


FIG. 15: A cosine-modulated Gaussian pulse becomes temporarily trapped in the potential well for the case $(\gamma, r_b, L) = (20, 250, 1)$. Initial data is chosen as $\psi = \cos(x) \exp[-(x - x_0)^2/2\sigma^2]$ centred at $x_0 = -20$ with a variance of $\sigma = 5$, moving to the right. In Fourier space this signal is a Gaussian centred about $\omega = 1$. We show the signal undergoing two reflections off the brane; the potential barrier at the photon-sphere partially reflects the signal resulting in a bouncing, temporary trapping of the wave.

brane signal which disappears and then reappears many times over—a state which looks like a collection of recurrent gravitons. This effect is shown in Fig. 16 for a long time integration.

The Fourier transform of this signal, Fig. 17, shows which modes dominate the waveform. The main curve shown the FT of the brane signal; the Gaussian is the FT of the initial data, and the inset shows the signal at very late times. We can easily discern the peaks in the spectrum which correspond to the spikes in η , shown in the inset of Fig. 13. Indeed, the signal in Fourier space looks very like (initial data) $\times \eta$, as expected from our Green’s function analysis. Note, however, the the lowest modes are far too narrow to resolve numerically ($\sim 10^{-10}$).

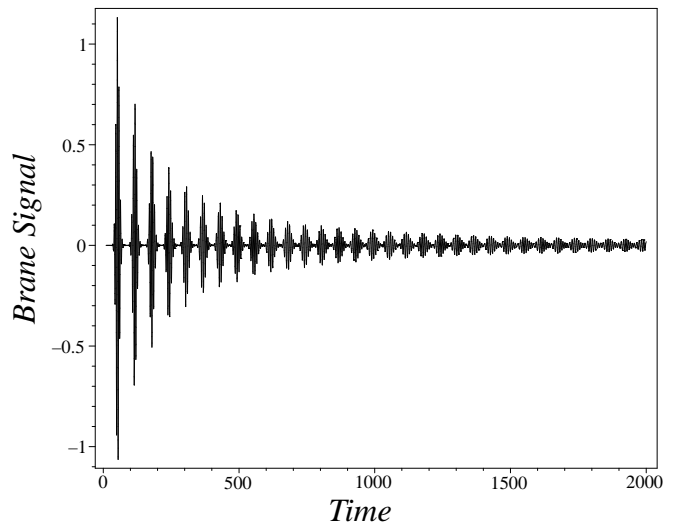


FIG. 16: The brane signal for the situation shown in Fig. 15. The gravitons appear in short bursts in this model, despite arising from a single coherent state in the bulk. Only at late times does this morph into what looks like ‘normal’ behaviour for gravity waves on a brane.

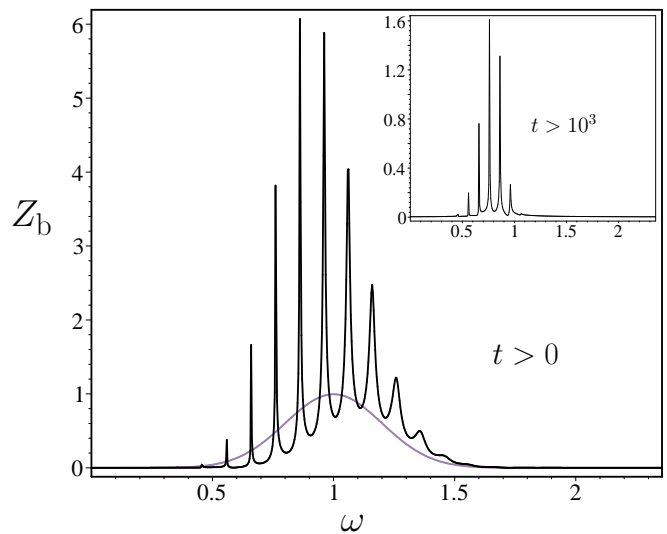


FIG. 17: Fourier transform of the brane signal in Fig. 16. The original signal is a Gaussian in Fourier space (grey curve), which gets combed into discrete frequencies over successive oscillations between the photon sphere and the brane. The very late time part of the signal is shown in the inset: the higher frequency components have a quicker damping time so only the lowest QNMs are left.

C. Steady state gravitational radiation: brane-black hole thermal equilibrium

Our last ‘initial value problem’ example does not really involve initial data at all. Consider a situation where the gravity waves near the horizon are a super position of

standing waves:

$$\psi(t, x) = \int d\omega Z_\infty(\omega) e^{i\omega t} \cos(\omega x + \delta), \quad x \rightarrow \infty. \quad (73)$$

This represents a situation where there is an equal amount of energy flux from and to the black hole. Physically, this is a good model of a brane in thermal equilibrium with the flux of Hawking radiation coming from the horizon. In that case, the power in the asymptotic waveform is given by the blackbody formula

$$|Z_\infty(\omega)|^2 = \frac{\omega^3}{e^{\omega/T_H} - 1}, \quad (74)$$

where the Hawking temperature is $T_H = \kappa/2\pi$ and κ is the surface gravity. Somewhat trivially, we use the definition of the trapping coefficient to obtain the brane signal

$$\psi_b(t) = \int d\omega \eta(\omega) Z_\infty(\omega) e^{i\omega t}, \quad (75)$$

and power spectrum

$$\frac{dE}{d\omega} = 4\pi^2 \xi(\omega) |Z_\infty(\omega)|^2 = \frac{4\pi^2 \xi(\omega) \omega^3}{e^{\omega/T_H} - 1}. \quad (76)$$

This result is pretty much identical to what we had from the Green's function answer for the scattering of a compact pulse: the power of the brane signal is the power in the waveform at infinity times $\xi(\omega)$. Hence, the same conclusion holds here: The blackbody spectrum is amplified at the positions of QBS frequencies, and that amplification has a Lorentzian lineshape whose width is proportional to the lifetime of the resonance.

VI. DISCUSSION

A. Summary of resonances

One of the main objectives of this paper was to gain complete knowledge of the quasi-normal resonances of Einstein-static braneworlds. Practically, this meant calculating QNM frequencies in different regions of the 3-dimensional (γ, r_b, L) parameter space characterizing the bulk gravity waves. Using two different numerical methods and a variety of analytic techniques, we managed to determine the behaviour of the resonant modes in a number of different interesting limits. In Fig. 18, we have summarized the key qualitative features of the resonances as a function of the model parameters.

Another way of presenting our results involves classifying resonances as over-damped ($\text{Im } \omega \gg \text{Re } \omega$), moderately damped ($\text{Im } \omega \sim \text{Re } \omega$), or under-damped ($\text{Im } \omega \ll \text{Re } \omega$). Then we can ask: Which parameter choices produce which type of resonance?

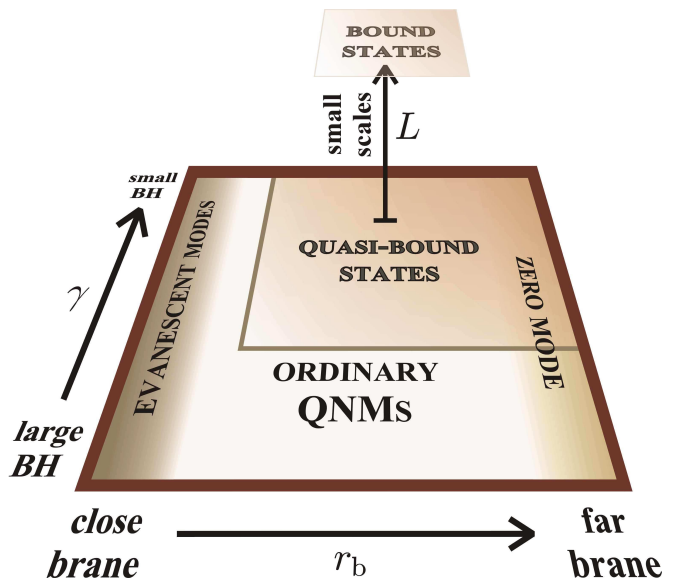


FIG. 18: Dominant resonant behaviour in different regions of the (γ, r_b, L) parameter space

Over-damped modes: Evanescent resonances occur when the brane is very close to the horizon – gravitons are sucked off the brane with great efficiency. In fact, when the brane is extremely close the concept of gravity waves is a bit dubious: all QNMs are purely imaginary, so no oscillations take place at all, and such modes just decay exponentially. For branes a bit further out there may be a small number QNMs with non-zero real part.

Moderately damped modes: When the brane is located at a moderate distance from the black hole, or the black hole is large so that no resonant cavity exists, we have the situation of ‘normal’ QNMs. This means that any signal will typically be dominated by the mode with the lightest damping – which also has the lowest frequency. This mode tends to dominate any signal very quickly. As discussed in detail in our previous work [3], all the resonant modes of pure tension branes are in this class.

Under-damped modes: Very long-lived modes arise in several different situations:

Zero-mode: For all (γ, L) , as $r_b \rightarrow \infty$ the fundamental mode becomes purely real, and matches the GR frequency; this mode is stuck to the brane. The higher overtones remain complex.

Quasi-bound states: When the black hole is small ($\gamma \gtrsim 2$) there exists a well in the potential; provided the brane is located past this well a pseudo-resonant cavity forms and QNMs with τ^2 less than the peak in the potential may

be interpreted as quasi-bound states. These modes have tiny imaginary parts implying a very long lifetime before they tunnel into the horizon.

Bound states: Quasi-bound states become bound on small scales: as $L \rightarrow \infty$, we have $\text{Im}(\omega)$ vanished exponentially quickly. This implies that on small scales an ES brane will look like a two brane model with virtually even spacing between all modes except the fundamental.

This list and Fig. 18 encapsulate our essential results on the quasi-normal modes of Einstein-static braneworlds.

B. The key role of the trapping coefficient in the initial value problem

An intriguing, and somewhat unexpected, by-product of our work has been the trapping coefficient η . Recall that this was originally introduced to help us calculate quasi-bound state frequencies when r_b became too large for the series method to handle. But in our Green's function analysis of the initial value problem in Sec. V A, $\eta(\omega)$ played a prominent role Fourier transform of the brane signal. Indeed, for the case of a compact pulse propagating towards the brane from infinity, the power spectrum on the brane was shown to be simply $\xi = \eta^2$ times the power spectrum of the pulse. In other words, the trapping coefficient tells us to what degree each Fourier component from $x = -\infty$ is localized on the brane.

In this sense, the precise functional form of $\xi(\omega)$ is crucial. To see how, assume for a moment that we only know the quasi-normal modes of the system and are ignorant of $\xi(\omega)$. Then, in any given scattering experiment we would predict that the brane power spectrum will be enhanced in some range $\Delta\omega \sim \Gamma_n$ around each resonant frequency ϖ_n ; but we would not know beforehand to what degree each mode would be excited by the initial data. This is a known conundrum in black hole perturbation theory [31]: quasi-normal modes by themselves only tell half the story, one also needs their 'excitation strengths' to really make detailed predictions.

However, using ξ to predict brane signal side-steps the whole issue because information about the excitation strengths is *already* encoded in the heights of the Lorentzian peaks representing the resonances. In small black hole/far brane cases ξ is a very spiky function, which means that it effectively combs initial data into a sum of lightly damped sinusoids centered about quasi-bound state frequencies, and efficiently suppresses the power in-between. Even when the QNMs are heavily damped the trapping coefficient plays an important role, amplifying signals in the region near the fundamental QNM, but suppressing signals of lower frequency. At the other end of the spectrum, ξ tells us in detail how high energy waves from the horizon are felt on the brane, a

subject on which quasi-normal modes have nothing to say.

But there are limitations to what can be learned in this fashion. If initial data has support outside the asymptotic region (i.e., close to the brane), things become muddled because our simple Green's function result for the scattering of distant pulses does not apply. The only sure thing in these cases comes from the quasi-normal modes, in that they still predict the position and width of resonant peaks in the brane signal. The actual power carried in each mode must be obtained by other means. Having stated that caveat, the trapping coefficient remains a powerful tool for describing the resonances of the Einstein-static braneworld. It has the attractive quality of being much easier to calculate than QNMs from a series solution, and it neatly communicates most of the important features of the scattering problem. We expect it will be of considerable use in other 'one-sided' brane scattering problems that feature lightly damped resonances and a flat asymptotic region.

C. Implications for cosmology and future work

Einstein-static branes become closed cosmological branes if we allow their radii to depend on time $r_b = a(t)$. The dynamics of $a(t)$ is governed by the Friedman equation (15). The evolution of gravity waves in the most general scenarios is more complicated than the static case considered in this paper, with a formal solution of the form

$$\psi_b(t) = \int dt' dx' G(t, x_b; t', x') \mathcal{I}(t', x'). \quad (77)$$

Here, G is the real space retarded Green's function and \mathcal{I} represents a generic source which includes $\psi(t, x)$ and perhaps other fields. Solving integro-differential equations of this type are the essential obstacle in braneworld cosmology [5, 32]. This is largely because the moving brane boundary condition makes it exceedingly difficult to deal with the Green's function in generic situations.

However, in the high-frequency regime we can make use of a multiple-scales approximation [17] to make some progress. This relies on the fact that if gravitational waves oscillate much faster than the brane moves, they will 'see' the brane to be stationary. To zeroth order in this approximation, the Green's function above is just the frequency space Green's function we developed in Sec. V transformed into the time domain. On dimensional grounds, 'slow' brane motion implies $\omega \gg H$, which means that our static results should apply to waves with oscillation periods much shorter than the Hubble time. Another way to state this is that the static Green's function is a good approximation to the moving Green's function provided $H(t - t') \ll 1$.

Hence, any quasi-normal modes we have found will be approximate resonant solutions to the moving brane problem if $\text{Re } \omega_n \gg H$. In this picture, one thinks of the

frequency of such modes as quantities evolving in time in a quasi-static, adiabatic process. Then, plots like Figs. 4 and 10, which show the variation of ω_n with r_b , can be re-interpreted as depicting the evolution of resonant frequencies with cosmological epoch, provided we only pay attention to the high frequency modes. Ideally, we would like to understand the systems resonances at lower frequencies, which would involve moving beyond the zeroth order static approximation to the the Green's function. An interesting future project would involve formalizing such an approximation scheme and then defining generalized, *dynamic* quasi-normal modes.

Finally, we note that due to the lack of time symmetry, it is more common in cosmology to characterize modes by their comoving wavelengths as opposed to their frequencies. For branes in the pure tension or far brane regimes, all resonances we found had $\text{Re } \omega_n > k$, as might be expected from the null momentum condition in 5 dimensions. Hence, our slow motion approximation can be re-cast in terms of spatial wavelengths: *on sufficiently sub-Hubble scales, gravity waves on a cosmological brane will be dominated by the quasi-normal resonances of the corresponding static brane.* Most importantly, this means that we recover a RS-like zero-mode for late cosmological epochs and on small scales. This is a critical test for the viability of braneworld cosmological modes involving a bulk black hole – if it were not true, we would see significant departures from general relativity over astrophysical distances in the current universe. However, it is tantalizing that we only find an *approximate* zero mode. This leaves the door open to finding small corrections to standard gravity induced by the presence of a bulk black hole. This is an important subject for future study.

Acknowledgments

CC is supported by PPARC and SSS is supported by NSERC. We would like to thank K Koyama, A Mennim, D Wands and especially R Maartens for many productive discussions on this work.

APPENDIX A: THE CLOSE BRANE LIMIT AND EVANESCENT MODES

In this appendix, we find an analytic solution to the master wave equation when the brane is close to the black hole horizon $r_b \sim 1$. The goal is to obtain an exact expression for the purely imaginary evanescent modes seen in Sec. III C for $r_b \rightarrow 1$.

The extreme close brane limit is defined by $r_b - 1 \ll 1$. Since $r \in (1, r_b)$, we have

$$f \approx 2\kappa(r - 1) \approx e^{2\kappa x} \ll 1, \quad (\text{A1})$$

in between the brane and the black hole horizon (recall that $\kappa = (2 + \gamma^2)/\gamma^2$ is the surface gravity). We expand

the wave equation (21) to leading order in $e^{2\kappa x}$, and apply a linear coordinate transformation $X = 2\kappa(x_b - x)$ to simplify matters. Assuming $\psi_k = e^{i\omega t} \Phi_{k\omega}(X)$, and defining the parameters

$$\Omega = \frac{\omega}{2\kappa}, \quad \Delta = \frac{3}{2} \left(1 - \frac{1}{r_b}\right),$$

$$\beta^2 = \frac{[6 + (L^2 + 2L + 3)\gamma^2](r_b - 1)}{2(2 + \gamma^2)}, \quad (\text{A2})$$

yields the simple wave equation

$$\Omega^2 \Phi_{k\omega}(X) = -\Phi_{k\omega}''(X) + \beta^2 e^{-X} \Phi_{k\omega}(X), \quad (\text{A3a})$$

$$\Phi_{k\omega}'(0) = -\Delta \Phi_{k\omega}(0). \quad (\text{A3b})$$

Note that the X coordinate has been selected such that the brane is at $X = 0$ and the horizon is at $X = \infty$. The ODE (A3a) has the following exact solution satisfying (A3b):

$$\Phi_{k\omega}(X) = F_1 I_\nu(2\beta e^{-X/2}) + F_2 K_{-\nu}(2\beta e^{-X/2}), \quad (\text{A4})$$

where $\nu = 2i\Omega$ and

$$F_1 = \beta K_{1-\nu}(2\beta) + (i\Omega + \Delta) K_\nu(2\beta), \quad (\text{A5a})$$

$$F_2 = \beta I_{1+\nu}(2\beta) + (i\Omega - \Delta) I_\nu(2\beta). \quad (\text{A5b})$$

Here, I_μ and K_μ are the modified Bessel functions of order μ . In order to find the quasi-normal frequencies, we need to know about the asymptotic behaviour of these Bessel functions near the horizon at $X = \infty$. From the relations [33]

$$I_\mu(2z) = \frac{z^\mu}{\mu!} \left[1 + \frac{z^2}{\mu + 1} + \mathcal{O}(z^4)\right], \quad (\text{A6a})$$

$$K_\mu(2z) = \frac{\pi}{2} \frac{I_{-\mu}(2z) - I_\mu(2z)}{\sin \pi \mu}, \quad (\text{A6b})$$

we deduce the large X behaviour

$$I_\nu(2\beta e^{-X/2}) \rightarrow \text{const.} \times e^{-i\Omega X}, \quad (\text{A7a})$$

$$K_{-\nu}(2\beta e^{-X/2}) \rightarrow \text{const.} \times \sin(\Omega X + \varphi), \quad (\text{A7b})$$

where φ is some constant (real) phase. We see that the former represents a purely outgoing wave at the horizon, while the latter is a mixture of incoming and outgoing radiation. To have a QNM, we need to set the contribution from the incoming radiation equal to zero. Hence, the quasi-normal frequencies are the (complex) $\omega = 2\kappa\Omega$ for which

$$F_2 = F_2(\omega; \gamma, r_b, L) = 0. \quad (\text{A8})$$

Notice that $r_b - 1 \ll 1$ means that β is a small parameter. Furthermore, for any given choice of γ and L , we see that Δ is of the same order as β^2 . Therefore, it makes sense to expand F_2 in powers of β . Again using (A6a), we find

$$F_2 = \beta^\nu \left[\frac{i\Omega}{\nu!} + \frac{\beta^2(1 + i\Omega)}{(1 + \nu)!} - \frac{\Delta}{\nu!} + \mathcal{O}(\beta^4) \right]. \quad (\text{A9})$$

To leading order in β , we find that $F_2 = 0$ implies $\Omega/\nu! = 0$, which has solutions

$$\Omega = 0, \quad \nu = -1, -2, -3 \dots \quad (\text{A10})$$

Expressing Ω and ν in terms of ω and κ yields:

$$\lim_{r_b \rightarrow 1} \omega_n = i\kappa n, \quad n = 0, 1, 2, 3 \dots \quad (\text{A11})$$

This simple formula holds for all γ and L . So, when the brane is very close to the horizon, the quasi-normal fre-

quencies are evenly spaced along the positive imaginary axis, in agreement with the results obtained from the series solution in Sec. III C. It is interesting to see that the QNM frequencies scale with the surface gravity of the black hole in this limit, just like the small- γ QNM frequencies of a S-AdS black hole [34] or the overtones of a pure tension Einstein-static brane [3]. Finally, we have quantitatively compared (A11) to our series solutions for the cases shown in Fig. 4 and found excellent agreement.

-
- [1] H.-P. Nollert, *Class. Quantum Grav.* **16**, R159 (1999).
[2] S. S. Seahra (2005), hep-th/0501175.
[3] S. S. Seahra, C. Clarkson, and R. Maartens (2005), gr-qc/0504023.
[4] L. Randall and R. Sundrum, *Phys. Rev. Lett.* **83**, 4690 (1999), hep-th/9906064.
[5] R. Maartens, *Living Rev. Rel.* **7**, 7 (2004), gr-qc/0312059.
[6] D. Langlois, R. Maartens, and D. Wands, *Phys. Lett.* **B489**, 259 (2000), hep-th/0006007.
[7] D. S. Gorbunov, V. A. Rubakov, and S. M. Sibiryakov, *JHEP* **10**, 015 (2001), hep-th/0108017.
[8] K. Koyama and K. Takahashi, *Phys. Rev.* **D68**, 103512 (2003), hep-th/0307073.
[9] K. Koyama and K. Takahashi, *Phys. Rev.* **D67**, 103503 (2003), hep-th/0301165.
[10] T. Kobayashi and T. Tanaka, *Phys. Rev.* **D69**, 064037 (2004), hep-th/0311197.
[11] K. Koyama and J. Soda, *Phys. Rev.* **D62**, 123502 (2000), hep-th/0005239.
[12] D. Langlois, R. Maartens, M. Sasaki, and D. Wands, *Phys. Rev.* **D63**, 084009 (2001), hep-th/0012044.
[13] J. D. Barrow and R. Maartens, *Phys. Lett.* **B532**, 153 (2002), gr-qc/0108073.
[14] B. Leong, P. Dunsby, A. Challinor, and A. Lasenby, *Phys. Rev.* **D65**, 104012 (2002), gr-qc/0111033.
[15] B. Leong, A. Challinor, R. Maartens, and A. Lasenby, *Phys. Rev.* **D66**, 104010 (2002), astro-ph/0208015.
[16] R. A. Battye, C. Van de Bruck, and A. Mennim, *Phys. Rev.* **D69**, 064040 (2004), hep-th/0308134.
[17] R. A. Battye and A. Mennim, *Phys. Rev.* **D70**, 124008 (2004), hep-th/0408101.
[18] K. Koyama, *JCAP* **0409**, 010 (2004), astro-ph/0407263.
[19] T. Kobayashi and T. Tanaka, *JCAP* **0410**, 015 (2004), gr-qc/0408021.
[20] T. Hiramatsu, K. Koyama, and A. Taruya, *Phys. Lett.* **B578**, 269 (2004), hep-th/0308072.
[21] K. Ichiki and K. Nakamura, *Phys. Rev.* **D70**, 064017 (2004), hep-th/0310282.
[22] K. Ichiki and K. Nakamura (2004), astro-ph/0406606.
[23] T. Hiramatsu, K. Koyama, and A. Taruya, *Phys. Lett.* **B609**, 133 (2005), hep-th/0410247.
[24] H. Kodama and A. Ishibashi, *Prog. Theor. Phys.* **110**, 701 (2003), hep-th/0305147.
[25] J. D. Barrow, G. F. R. Ellis, R. Maartens, and C. G. Tsagas, *Class. Quant. Grav.* **20**, L155 (2003), gr-qc/0302094.
[26] J. P. Gregory and S. F. Ross, *Phys. Rev.* **D64**, 124006 (2001), hep-th/0106220.
[27] J. R. Taylor, *Scattering Theory* (Wiley, New York, 1972).
[28] L. D. Landau and E. M. Lifshitz, *Quantum Mechanics (Non-relativistic theory)*, vol. 3 of *Course of Theoretical Physics* (Elsevier, London, 1977), 3rd ed.
[29] S. Chandrasekhar and V. Ferrari, *Proc. Roy. Soc. Lond.* **A432**, 247 (1991).
[30] Y. Kojima, N. Andersson, and K. D. Kokkotas, *Proc. Roy. Soc. Lond.* **451**, 341 (1995), gr-qc/9503012.
[31] N. Andersson, *Phys. Rev.* **D55**, 468 (1997), gr-qc/9607064.
[32] S. Mukohyama, *Phys. Rev.* **D64**, 064006 (2001), hep-th/0104185.
[33] G. B. Arfken and H. J. Weber, *Mathematical Methods for Physicists* (Academic, New York, 1995), 4th ed.
[34] G. T. Horowitz and V. E. Hubeny, *Phys. Rev.* **D62**, 024027 (2000), hep-th/9909056.